California State University, Northridge

Battling Antibiotic Resistance by Investigation of *Acinetobacter baumannii* Enoyl Acyl Carrier Protein Reductase

A thesis submitted in partial fulfillment of the requirements

For the degree of Master of Science in Biochemistry

By

Casper Wong

December 2017

The thesis of Casper Wong is approved:

Dr. Karin Crowhurst	Date
Dr. Paula Fischhaber	Date
Dr. Jessica Vey, Chair	Date

California State University, Northridge

Acknowledgments

The research program was a difficult and meaningful experience. My parents, Kam and Melinda Wong, and fiancée, Shirley Yan, supported me throughout the process. I would like to thank my mentor and principal investigator Dr. Jessica Vey for giving me an opportunity to grow as a research student in her laboratory. I would also like to acknowledge the other graduate students from the lab, Charmaine Ibarra, Liliana Gonzalez-Osorio, Kellee Johnson, and Samatar Jirde, for their guidance and assistance.

Table of Contents

List of Figures

List of Tables

List of Abbreviations

abFabI	*Acinetobacter baumannii* enoyl acyl carrier protein reductase
ACP	acyl carrier protein
CBP	cell break pellet
CBS	cell break supernatant
DH	dehydrase
ecFabI	*Escherichia coli* enoyl acyl carrier protein reductase
ER	enoyl reductase
FabI	enoyl acyl carrier protein reductase
FAS-I	fatty acid biosynthesis I
FAS-II	fatty acid biosynthesis II
FPLC	fast protein liquid chromatography
HIC	hydrophobic interaction chromatography
InhA	*Mycobacterium tuberculosis* enoyl acyl carrier protein reductase
IPTG	isopropyl β-D-1-thiogalactopyranoside
kDa	kilodalton(s)
KR	ketoacyl reductase
KS	ketoacyl synthase
MAT	malonyl/acetyltransferase
MDR-TB	multidrug-resistant tuberculosis
MW	molecular weight
NADH	nicotinamide adenine dinucleotide
NADPH	nicotinamide adenine dinucleotide phosphate

NDT	2-(Toluene-4-Sulfonyl)-2H-Benzo[D][1,2,3]Diazaborinin-1-ol
Ni-NTA	nickel nitrilotriacetic acid
OD_{600}	optical density at 600 nanometers
pI	isoelectric point
RMSD	root-mean-square deviation
saFabI	*Staphylococcus aureus* enoyl acyl carrier protein reductase
SBL	substrate binding loop
SDS-PAGE	sodium dodecyl sulfate polyacrylamide gel electrophoresis
TEMED	tetramethylethylenediamine
TS	thioesterase
vlmH	isobutylamine N-hydroxylase
w/v	weight/volume
XDR-TB	extensively drug-resistant tuberculosis

Abstract

Battling Antibiotic Resistance by Investigation of *Acinetobacter baumannii* Enoyl Acyl Carrier Protein Reductase

By

Casper Wong

Master of Science in Biochemistry

Bacterial resistance to currently available antibiotics is becoming a major public health concern. *Acinetobacter baumannii* is a Gram-negative bacterial species that ranks among the top antibiotic resistant pathogens. It infects compromised immune systems in humans and is a major cause of hospital infections. Narrow spectrum antibiotics need to be developed to specifically target and eliminate *A. baumannii*. An effective way to eliminate bacteria is by inhibiting the synthesis of fatty acids needed to build the cell membrane necessary for bacterial survival. Since humans use the fatty acid biosynthesis I pathway while bacteria use the fatty acid biosynthesis II pathway, it is safe to inhibit proteins in the fatty acid biosynthesis II pathway without affecting humans. Our therapeutic target is the enoyl acyl carrier protein reductase (FabI), which catalyzes the final step of the elongation cycle in the fatty acid biosynthesis II pathway. FabI is needed to reduce the double bond of the fatty acid being elongated in the pathway. Inhibition of FabI in *A. baumannii* will prevent the bacteria from generating fatty acids and lead to their demise. Here, the purification of soluble and active *Acinetobacter baumannii* enoyl acyl carrier protein reductase (abFabI) and initial rate kinetics of abFabI with inhibitors

are described. Various chromatography methods were used to purify abFabI, and NADH consumption assays were performed at 340 nm to monitor abFabI activity. A shorter sequence (abFabI-a) and a longer sequence (abFabI-b), both designated abFabI in the literature, are also compared here, with abFabI-b including an N-terminal addition that we postulate to be a result of a sequencing error. abFabI-a was found to be homotetrameric and active while abFabI-b was misfolded and inactive. The purified active abFabI-a was used to determine IC_{50} values for known FabI inhibitors triclosan, four examples of compound from the diazaborine class, and isoniazid. Triclosan inhibited abFabI with an IC_{50} value of 0.486 μM, which was comparable to the IC_{50} values of triclosan on FabI homologs. Diazaborines 14b and 35b inhibited abFabI with IC_{50} values of 5.81 and 173 μM, respectively. In contrast, diazaborines 18c and 39 and isoniazid were not able to inhibit abFabI. Successful abFabI inhibition by triclosan and diazaborines 14b and 35b enables future development of narrow spectrum antibiotics by using these compounds for structure-based design.

Chapter 1

Introduction

Research Significance

Impacts of Increasing Bacterial Resistance to Antibiotics on Human Health

Bacterial resistance to first-line and second-line antibiotics is an increasing public health concern.[1] These most heavily used antibiotics are becoming progressively less effective against various resistant bacteria. For example, amoxicillin is a first-line penicillin antibiotic that is losing effectiveness against *Helicobacter pylori*, a bacterial species that causes gastric ulcers and gastritis, due to an increased bacterial resistance to antibiotics.[2] *Mycobacterium tuberculosis*, a bacterial species that causes tuberculosis was successfully treated with first-line antibiotics called isoniazid and rifampicin, but the emergence of multidrug-resistant tuberculosis (MDR-TB), which has resistance to both isoniazid and rifampicin, led to treatment with second-line drugs such as amikacin, kanamycin, and capreomycin.[3,4] By becoming resistant to the first- and second-line drugs, MDR-TB can develop into extensively drug-resistant tuberculosis (XDR-TB), against which there are even fewer effective drugs. Even the carbapenem antibiotic class, which is currently the final line of antibiotics used for infections caused by multidrug-resistant bacteria, are becoming ineffective against pathogens like *Acinetobacter baumannii*.[5] Since bacterial infections are posing a threat to health once again, new strategies are needed to overcome the emergence of drug-resistant bacteria.[6]

Multidrug Resistance in Modern *A. baumannii*

As of 2017, *Acinetobacter baumannii* has become one of three World Health Organization's highest priority pathogens, which are ranked as the most critical pathogens for which research and development of new antibiotics is necessary.[5] Limited options for treating infections caused by the multidrug-resistant *A. baumannii* highlights an urgent need for development of novel therapeutics by newer methods.[7] A better understanding of *A. baumannii* is needed in order to more effectively target and eliminate it. *A. baumannii* is a Gram-negative bacteria that acts as an opportunistic pathogen, attacking moist areas, like wounds, and infecting compromised immune systems. *A. baumannii* infections are found all over the world and cause many hospital outbreaks that lead to clinical problems such as pneumonia, bloodstream infections, urinary tract infections and meningitis.[1,7,8] Multidrug resistant *A. baumannii* is a critical target because there may be research in progress for finding novel treatments for infections caused by *A. baumannii*, but there are currently no promising treatments publicly available.[9] The surge of bacterial resistance that we have observed in the last few decades calls for immediate action to find new working drugs.

Narrow vs Broad Spectrum Antibiotics for Treatment of *A. baumannii*

One promising approach to tackling multidrug resistant *A. baumannii* is to develop narrow spectrum antibiotics that specifically treat it. Narrow spectrum antibiotics are selectively active against the bacterial species of interest. This type of antibiotic contrasts with broad spectrum antibiotics, which inhibit multiple bacterial species with less specificity. Both types of antibiotics are necessary in our therapeutic arsenal, as

broad spectrum antibiotics can be used to treat multiple bacterial species while narrow-spectrum antibiotics can target one and avoid the negative consequences of killing off beneficial bacteria in the body. Our focus is on enabling narrow spectrum antibiotic development by exploiting specific details that are unique to *A. baumannii* as compared to other bacterial species. To develop narrow spectrum antibiotics for *A. baumannii*, potential antibiotic targets need to be characterized in detail.

FAS-II as a Target for Narrow Spectrum Antibiotics

Our target for finding narrow spectrum antibiotics is an enzyme in the fatty acid biosynthesis II (FAS-II) pathway. When we inhibit distinct enzymes in the FAS-II pathway, bacteria cannot produce fatty acids that make up their cell membranes. Without the production of fatty acids, bacteria cannot maintain their cell membranes, which are vital for transporting molecules in and keeping unwanted molecules out. Abrogating fatty acid biosynthesis can therefore impair cell division and possibly lead to cell death. This makes the FAS-II pathway an appealing target for novel narrow spectrum therapeutics against *A. baumannii*.

Biological Context of Enoyl Acyl Carrier Protein Reductase (FabI)

Fatty Acid Biosynthesis Pathway

There are two major fatty acid biosynthesis pathways: fatty acid biosynthesis I (FAS-I) pathway used by humans and the FAS-II pathway used by bacteria. Both pathways utilize enzymes to synthesize fatty acids from acetyl CoA through a cyclic process that includes an initiation, elongation, and termination phase (Figure 1).[10] The

two pathways start with the initiation phase, where acetyl CoA is carboxylated to form malonyl CoA, followed by the elongation phase. Even though the elongation steps in both pathways are mechanistically the same, there are significant differences between the two. Most relevant to this work, the FAS-I pathway uses a large multi-enzyme protein complex called fatty acid synthase to grow the fatty acid chain in length, but the FAS-II pathway uses distinct enzymes to catalyze each reaction step to make the fatty acid chain. The existence of two pathways is advantageous because inhibiting specific enzymes in the FAS-II pathway used by bacteria generally will not affect the FAS-I pathway used by humans since the enzymes in their respective pathways are not identical, making the bacterial enzymes selective drug targets.[11,12] Even though the FAS-II pathway has many enzymes that can be exploited as targets for antibiotics, the enzyme of interest for this project is the enoyl acyl carrier protein (ACP) reductase, which is abbreviated FabI, specifically from *A. baumannii* (abFabI).

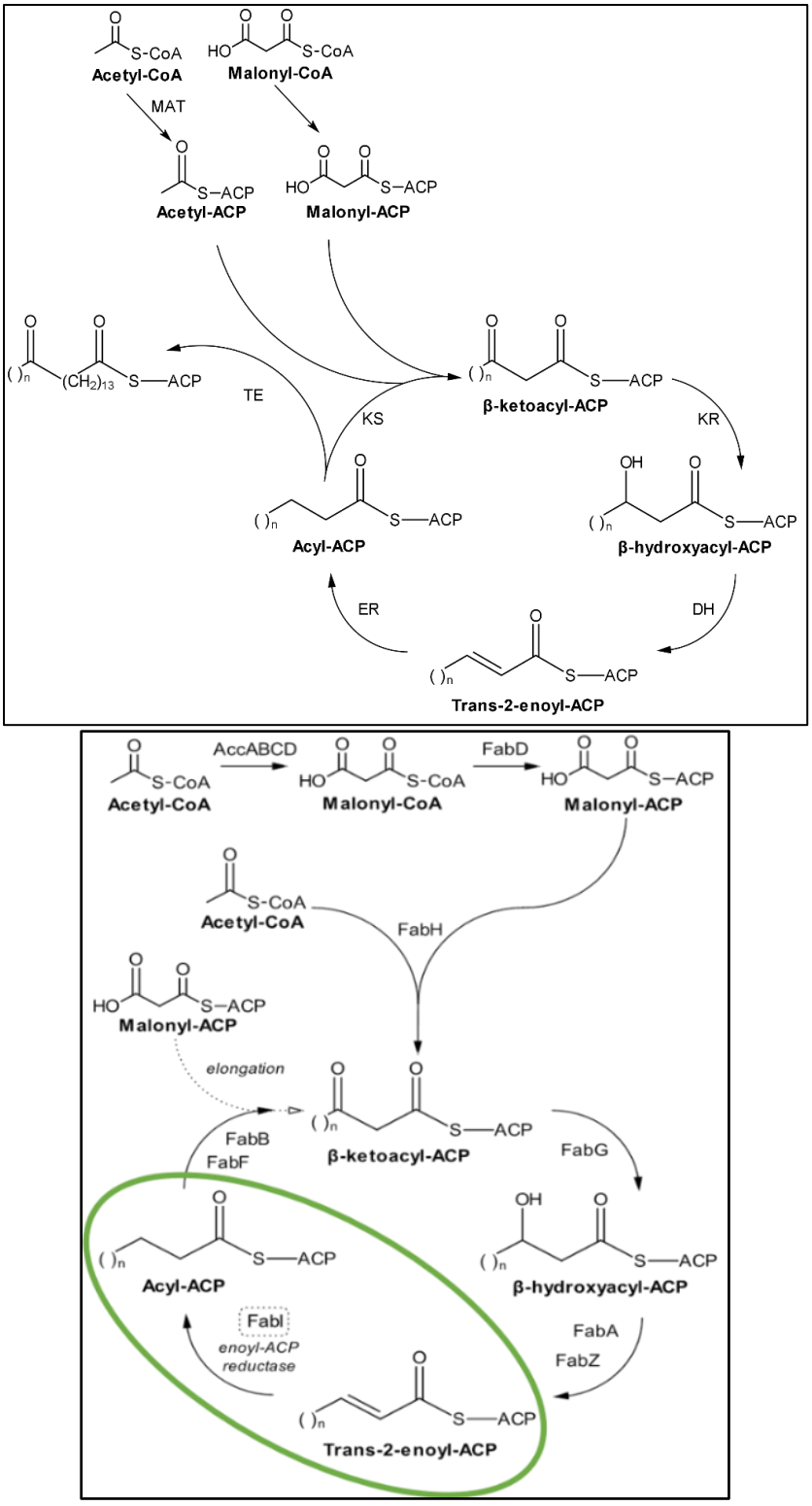

Figure 1: The fatty acid biosynthesis I and II pathways. FAS-I pathway is shown on the top and FAS-II pathway is shown on the bottom. The reduction step catalyzed by FabI is circled in green. Abbreviations in the FAS-I pathway: malonyl/acetyltransferase (MAT), ketoacyl synthase (KS), ketoacyl reductase (KR), dehydrase (DH), enoyl reductase (ER), and thioesterase (TE).

Mechanism of the Reduction Step Catalyzed by FabI

FabI is the enzyme used in the final step of the elongation phase in the FAS-II pathway. The enzyme catalyzes the reduction of trans-2-enoyl-ACP to acyl-ACP. This is a critical step in which either the fatty acid enters another round of the elongation phase or else it enters the termination phase in which the fatty acid chain is finally released. FabI reduces the trans double bond of the nascent fatty acid via electron donation from a nicotinamide cofactor. The C2-C3 double bond is reduced to a single bond (Figure 2).[12]

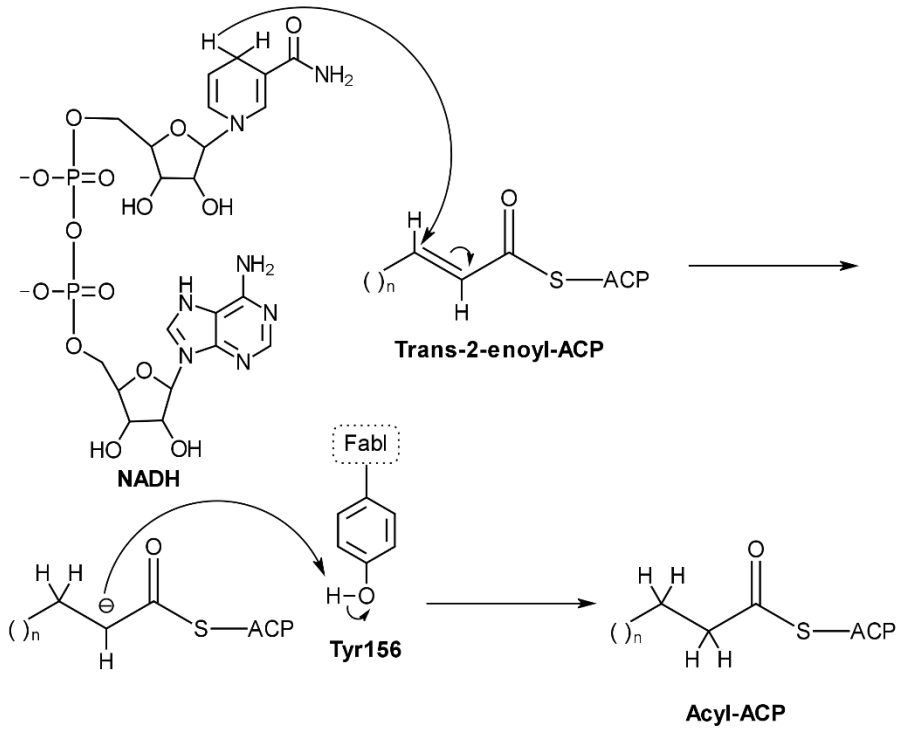

Figure 2: Mechanism of reduction step catalyzed by FabI.

The mechanism of the enoyl ACP reductases has been elucidated using the enzyme from *E. coli*. A hydride ion from NAD(P)H is transferred to the C3 of the trans-2-enoyl-ACP. This is followed by protonation of the resulting carbanion on C2 of the substrate by Tyr156 in ecFabI. Tyr156 is reprotonated by solvent via Lys163 in ecFabI to return the enzyme to its active form for another round of catalysis.[13] This NAD(P)H-

dependent mechanism by FabI is known in *E. coli*, but other bacterial species like *Mycobacterium tuberculosis* and *Staphylococcus aureus* are thought to use the same mechanism. Though a conserved mechanism is used, FabI of different species vary in several key ways; for example, the shape of the substrate binding pocket likely differs between FabI homologs and can change to accommodate the increasing fatty acid chain length. These differences in the substrate binding pocket can be exploited for narrow spectrum drug design because the enzyme deriving from a single bacterium of interest will have a unique binding pocket, thus, drugs can be developed to only target that specific bacterium. Detailed research must be carried out on FabI homologs from different species in order to elucidate these differences.

FabI Homologs Have Been Previously Exploited as Therapeutic Targets

FabI from various bacterial species have been studied as narrow-spectrum drug targets. Such studies have led to new drugs to battle antibiotic resistance and eradicate the selected bacterial species, like the novel scaffold benzimidazole-based inhibitors that inhibit saFabI and pyridone inhibitors that inhibit InhA.[14,15] Some notable therapeutics currently used to inhibit bacterial FabI include the diazaborines, triclosan, and isoniazid. Since the FabI active site varies depending on the bacterial species (Table 1 and Figure 3), the effectiveness of these therapeutics against specific bacterial species also varies.

Enzyme	RMSD with abFabI	Sequence Identity to abFabI
ecFabI	0.551 Å	63%
InhA	0.960 Å	30%

Table 1: Root-mean-square deviation (RMSD) and sequence identity between abFabI and FabI of other bacterial species. ecFabI (PDB ID: 5CFZ) and InhA (PDB ID: 4TRM) were compared to abFabI (PDB ID: 4ZJU).

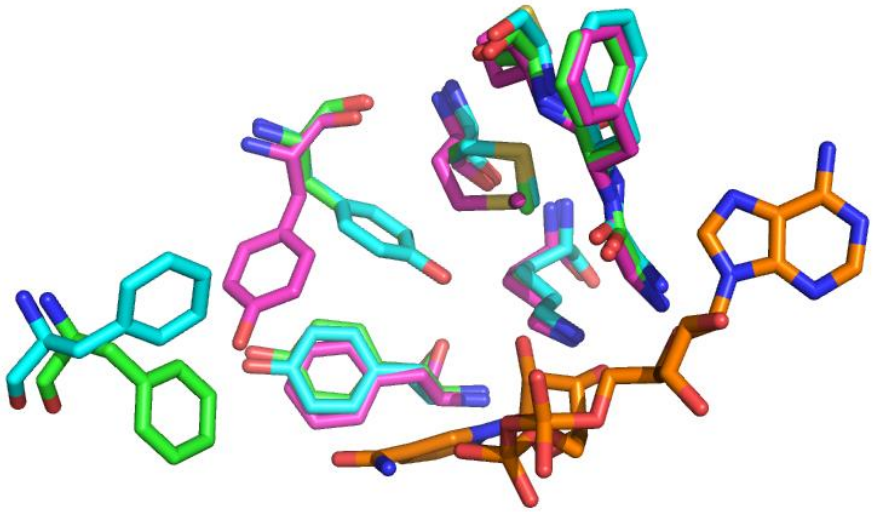

Figure 3: Superimposed FabI active sites. The FabI structures shown here are in the same states. The active site residues of abFabI in green (PDB ID: 4ZJU, ecFabI in blue (PDB ID: 5CFZ) and InhA in magenta (PDB ID: 4TRM) overlay relatively well but each active site still contains their own differences. NAD^+ is shown in orange.

It is essential to understand structure and function relationships in the active site of each FabI homolog in order to assist in drug design. FabI homologs from fifteen bacterial species have been structurally characterized (Table 2), but only a handful of them are biochemically characterized.

Bacterial Species	Year	Representative PDB ID
Brassica napus	1995	1ENO[16]
Mycobacterium tuberculosis	1995	1ENY[17]
Escherichia coli	1999	1QSG[18]
Plasmodium falciparum	2002	1NHG[19]
Aquifex aeolicus	2007	2P91[20]
Bacillus anthracis	2007	2QIO[21]
Helicobacter pylori	2007	2PD3[22]
Mycobacterium leprae	2007	2NTV[23]
Bacillus cereus	2010	3OJE[24]
Staphylococcus aureus	2010	3GNS[25]
Candidatus Liberibacter asiaticus	2013	4NK4[26]
Pseudomonas aeruginosa	2013	4NQZ[27]
Burkholderia pseudomallei	2014	4BKU[28]
Chlamydia trachomatis	2014	4Q9N[29]
Acinetobacter bauamnnii	2015	4ZJU[30]

Table 2: FabI of bacterial species that have been structurally characterized.

Currently known details about the enzyme are mainly from three bacterial species that have been extensively studied: *E. coli*, *M. tuberculosis*, and *S. aureus*. Our current understanding of catalysis by FabI is derived from studies on enoyl ACP reductase from *E. coli* (which will be referred to herein as ecFabI), which has been examined by structural characterization, functional studies, and kinetics experiments by several independent research groups.[18,31-36] FabI from *E. coli* was the enzyme used in seminal experiments showing that FabI is part of the FAS-II pathway.[31] ecFabI has been structurally characterized in its apo form and holo form with NAD^+ and inhibitors, like triclosan and diazaborines.[34] InhA, the enoyl ACP reductase of *M. tuberculosis*, has the largest number of crystal structures (78 total structures) registered out of the enoyl ACP reductase structures in the Protein Data Bank. Both triclosan and isoniazid have been shown to inhibit InhA.[33] The structure that was most recently solved out of these three species is the enoyl ACP reductase of *S. aureus* (saFabI). The number of structural investigations of saFabI have exploded since the first reported structure in 2010, yielding 27 total protein structures. Triclosan has also been shown to inhibit saFabI.

Structural Information of FabI Homologs May Suggest the Cause of Antibiotic Resistance

FabI homologs are similar in sequence, but the structure of their active sites may vary depending on the species. Bacterial FabI homologs all adopt a homotetrameric fold in which each monomer has its own active site and substrate binding loop (Table 3). The unique size, shape, flexibility, and architecture of each respective active site result in different effects with an inhibitor.

Enzyme	MW of Monomer (kDa)	MW of Homotetramer (kDa)
ecFabI	27.9	112
InhA	28.5	114
saFabI	28.0	112
abFabI	28.6	114

Table 3: Molecular weights of FabI monomers and homotetramers.

Most of our FabI structural information comes from inhibitor-bound structures of the enzyme from different bacterial species. Since many structures of ecFabI have been solved, details from ecFabI (PDB ID: 5CFZ[32], 1DFG[35], and 1D8A[37]) will be used to illustrate the active site of the FabI homologs. The active site includes key residues Gly93, Phe94, Ala95, Tyr146, Tyr156, Met159, Lys163, and Phe203 that are needed for substrate or inhibitor binding and function (Figure 4).

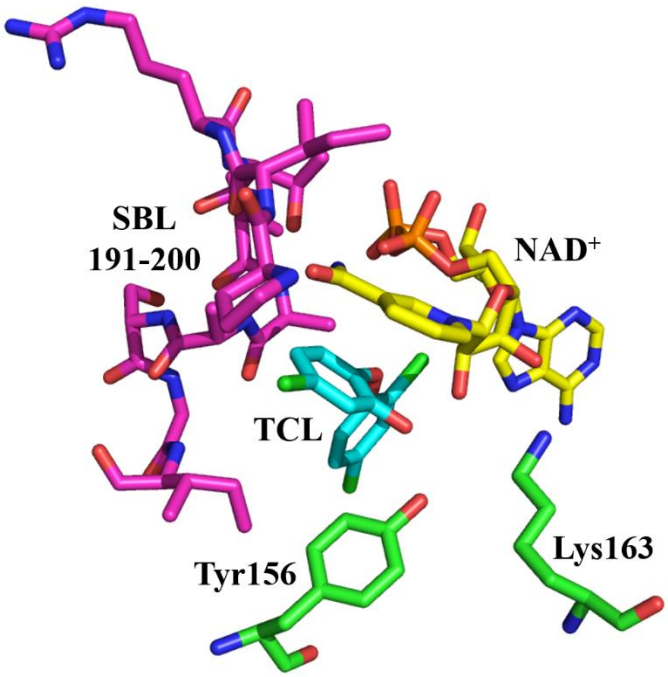

Figure 4: Active site of ecFabI. Catalytic residues of the ecFabI active site are shown in green (PDB ID: 1D8A). Triclosan is in cyan, NAD^+ is in yellow, and the substrate binding loop is in magenta. The rest of the active site residues have been excluded for a clear view of triclosan.

Tyr156 and Lys163 are the critical catalytic residues that are part of the double bond reduction step. Gly93, Phe94, Ala95, Tyr146, Tyr156, Met159, and Phe203 are

implicated in inhibitor binding, which suggests that they form the substrate binding surface since the inhibitors are competitive inhibitors. Phe203 is also part of the substrate binding loop (SBL), which is a distinct region that can undergo conformational change upon inhibitor binding. Mutations involving residues in the active site are believed to be one of the main causes of antibiotic resistance and also a reason that some bacterial species, such as *A. baumannii*, have evolved to include particular mutations to become less susceptible to the current therapeutics.

Use of Inhibitor-Bound FabI Structures in Rational Design and Drug Development

Crystal structures of ecFabI and InhA were reported more than two decades ago, and structures with various inhibitors bound to ecFabI and/or InhA have since been solved to help guide rational drug design efforts.[17,38] Inhibition studies on saFabI began around the year 2000, but the structure was not characterized until a decade later.[25,39] The three most widely-studied FabI inhibitors are the diazaborines, isoniazid, and triclosan, (Figure 5).

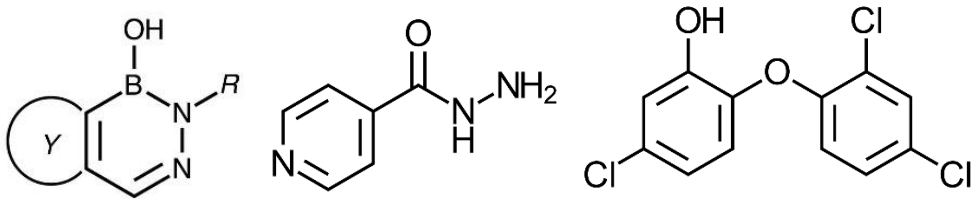

Figure 5: Structures of the diazaborine scaffold, isoniazid, and triclosan. The compounds are listed from left to right. Y is a fused five- or six-membered ring and R is a sidechain in the diazaborine scaffold.

The drugs are selective for the FabI of certain bacterial species due to slight differences in the FabI active site structure between bacterial species. IC_{50} and MIC are two parameters used to report inhibition. An IC_{50} value is the half maximal inhibitory

concentration, which is the concentration of an inhibitor that gives rise to a 50% decrease in enzyme activity. MIC is the minimum inhibitory concentration, which is the concentration of an inhibitor that prevents visible bacterial growth. The parameters have been reported for inhibitors on various FabI homologs. In order to fully exploit the differences in the active site for narrow-spectrum drug design, multiple structures with different inhibitors bound should be determined for each FabI homolog. These structures would provide comprehensive structural details for drug design, such as catalytic active site residues and conformational changes due to substrate or inhibitor binding.

Inhibition of FabI by Diazaborines

Diazaborines are chemical compounds that contain a scaffold comprising a phenyl ring connected to a diazaborinane that includes two nitrogen atoms and a boron atom bonded to a hydroxyl group (refer to Figure 4). This series of molecules, which differ in their substitution pattern (at x/y/z positions) inhibit FabI by forming a covalent complex with NAD^+ that binds tightly to the FabI active site. The complex of ecFabI, diazaborine, and NAD^+ (Figure 6) has already been structurally characterized by X-ray crystallography.[34,36,40]

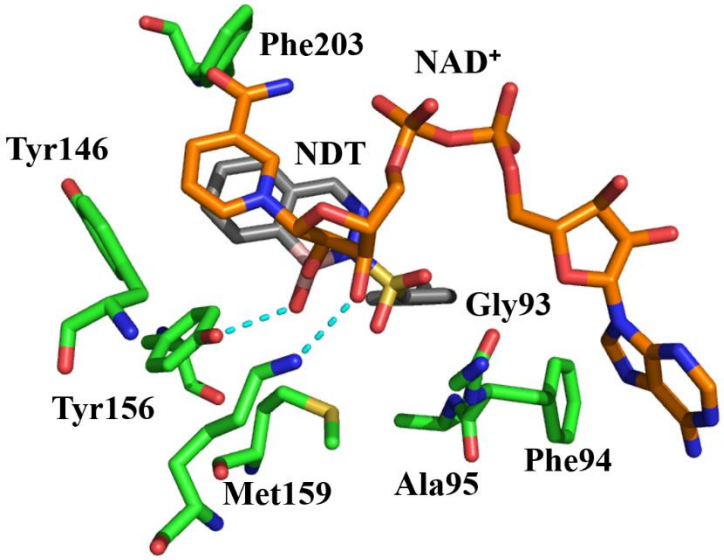

Figure 6: Structure of ecFabI-diazaborine-NAD$^+$. Active site residues are shown in green. The bicyclic ring of the diazaborine (gray) 2-(Toluene-4-Sulfonyl)-2H-Benzo[D][1,2,3]Diazaborinin-1-ol (NDT) stacks with the NAD$^+$ (orange) nicotinamide ring and also makes contact with Tyr146 and Tyr156 of ecFabI (green) through hydrogen bonds and van der Waals interactions. The boron atom of diazaborine is covalently bound with the 2′-OH of NAD$^+$.[35] Hydrogen bonds are shown in cyan. The structure is from PDB ID: 1DFG.

The boron atom of the diazaborine forms a covalent bond to the 2′-hydroxyl group of the nicotinamide ribose, while the bicyclic ring of the diazaborine π-stacks with the nicotinamide ring.[35] Diazaborine inhibition occurs by forming a tight complex with ecFabI and the nicotinamide cofactor.[35,41] To further strengthen the binding of the complex, the hydrogen of the phenol group from the Tyr156 in ecFabI hydrogen bonds with the hydroxyl group of the diazaborine. Besides Tyr156, other specific residues in the active site of ecFabI are involved in hydrogen bonding and steric hindrance that affect diazaborine inhibition.

A conformational change in the SBL also occurs upon binding of diazaborine molecules. The SBL in ecFabI (residues 190-207) is disordered in the apoenzyme and the NAD$^+$-bound form. It is not until diazaborine binds the enzyme to form a complex that

the loop becomes ordered.[42] When the loop becomes ordered as compared to its original disordered conformation, it forms a helical structure that reduces solvent accessibility and draws the SBL closer to the diazaborine. This is evident through the conserved residues Ala196 and Ala197 being drawn closer to diazaborine for van der Waals interactions; Thr194 is also now within distance for hydrogen bonding with the nicotinamide after ordering of the loop. The ordering makes the complex bind tighter and results in stronger inhibition. Mutations and conformational changes affect diazaborine binding, which may strengthen inhibition or lead to resistance of the drug.

Mutagenesis information can help illustrate how the active sites vary between FabI homologs, which makes FabI a good narrow-spectrum target. Gly93 is the most investigated residue of ecFabI associated with diazaborine inhibition, and mutations to this residue are associated with antibiotic resistance because diazaborine binding and inhibition requires the flexible glycine residue at this position. Site-directed mutagenesis has been performed on this specific residue to elucidate its function. When Gly93 was substituted with amino acids with small side-chains that are slightly larger than glycine, like alanine, ecFabI became resistant to diazaborine due to steric hindrance at the enzyme's binding site; when large side-chains, like arginine, were substituted for Gly93, the enzyme was completely inactivated.[40] Mutations that disrupt the substrate or inhibitor binding site, such as a smaller residue being substituted with a larger residue that extends into the binding site, can confer resistance to the inhibitor. Gly93Val, Met159Thr, and Phe203Leu exemplify this resistance strategy. The mutations disrupt the formation of a tight ecFabI-diazaborine-NAD(H) complex that is needed for optimal inhibition.

The IC_{50} and MIC values of diazaborine against FabI homologs (Table 4) can vary in efficacy and potency depending on which diazaborine is used because diazaborine compounds do not have the same exact structure even though they share the same scaffold. Active site and SBL differences of FabI homologs can be exploited for different binding affinities using different diazaborines to develop narrow spectrum therapeutics.

Diazaborine	Structure	Species	IC_{50} (µM)	MIC (µg/mL)
DZB	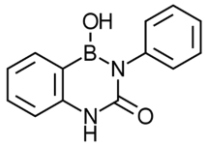	*M. tuberculosis*	>1000 [43]	
2-Propylsulfonyl-thienodiazaborine	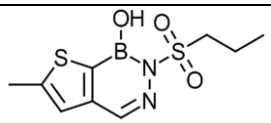	*E. coli* *K. pneumoniae* *S. typhimurium*		1.25 [44] 0.39 [44] 1 [45]
14b	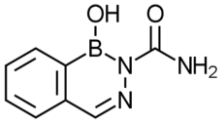	*E. coli* *M. smegmatis*		16 [46] >32 [46]

Table 4: IC_{50} and MIC values on different bacterial species by diazaborines.

Inhibition of FabI by Triclosan

Triclosan binds to ecFabI in the active site, in a similar location and position as observed with the diazaborines. Triclosan is a broad spectrum inhibitor that has been shown to inhibit many FabI homologs such as ecFabI, InhA, and saFabI (Table 5).

Bacterial species	IC_{50} (µM)	MIC (µg/mL)
E. coli	0.04 [33]	0.25 [32]
M. tuberculosis	1 [47]	5 [48]
S. aureus	3 [17]	0.25 [17]

Table 5. Inhibition parameters of triclosan with FabI from various bacterial species.

Inhibition of these three different enzymes by triclosan varies, and equivalent mutations made to each enzyme have different effects on triclosan affinity. The variability observed with respect to triclosan inhibition between the species lends

credence to the idea that FabI is a good narrow-spectrum target. Triclosan is a broad spectrum drug, but it could potentially be structurally modified to develop narrow spectrum derivatives. Triclosan is a competitive inhibitor of substrate binding and forms a complex with the enzyme and NAD^+ that prevents the enzyme from binding the substrate by occluding the binding site (Figure 7). The phenol ring of triclosan π-stacks with the nicotinamide ring of the NAD^+ cofactor.[18,33,34,37] Triclosan, like the diazaborines, is a tight binding inhibitor of ecFabI and the nicotinamide cofactor upon complex formation via hydrogen bonding.[18,33,34,37,49]

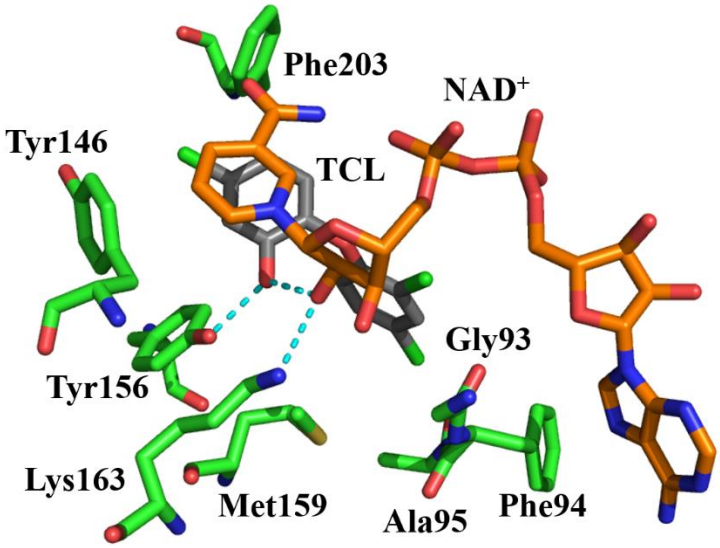

Figure 7: Structure of ecFabI-triclosan-NAD^+ complex. Active site residues are shown in green. Triclosan (gray), abbreviated TCL, has its hydroxychlorophenyl ring stacked with the nicotinamide ring of NAD^+ (orange). The hydroxyl group of triclosan is hydrogen bonded (cyan) with Tyr156 and the 2′-OH of the NAD^+. Lys163 is hydrogen bonded with the 2′-OH of the NAD^+. The structure is from PDB ID: 1D8A.[37]

As would be expected, many of the same amino acids involved in diazaborine binding are critical for the complex formation with triclosan as well. Tyr156, triclosan, and NAD^+ form a stable ternary complex by hydrogen bonding.[18,33,34,37,42] A loop region at residues 196-205 is disordered when bound with NAD^+ as a binary complex but becomes ordered

when triclosan binds and forms the ternary complex.[33] Ile192 to Ser198 has also been shown to form a loop that flips between an open and a closed conformation; the closed conformation is very important for improving the potency of triclosan binding.[49] The loop conformations and flexibility impact inhibitor affinity, which again lends credence to the use of FabI as a narrow-spectrum target.

Mutagenesis of Gly93, Met159, and Phe209 in ecFabI Affects Triclosan Affinity

Mutations to Gly93, Met159 and Phe203 were investigated to see if they correlate with triclosan resistance because these active site residues were shown to impact ecFabI's affinity for diazaborine.[42] Gly93Val, Met159Thr, and Phe203Leu mutations were subsequently shown to impact triclosan binding affinity, either preventing (Gly93Val) or weakening (Met159Thr and Phe203Leu) the binding of triclosan.[18,34,50] As proposed with respect to diazaborine, Gly93Val appears to create steric hindrance and disrupted the hydrogen bond interaction between Lys163 and the 2′-hydroxyl group of the nicotinamide ribose, which, in turn, prevents binding of triclosan. Interestingly, the Met159Thr mutation resulted in the opposite effect for triclosan binding compared to the increase in diazaborine binding affinity. The binding affinity of triclosan decreased, presumably due to the threonine side chain being shorter than the methionine side chain, which means less hydrophobic interactions and weaker binding between ecFabI and triclosan. Phe203 is part of the hydrophobic pocket and forms hydrophobic interactions with triclosan, so the removal of the phenylalanine side chain with the Phe203Leu

mutation caused a decrease of the triclosan binding affinity, which is identical to the effect of the lowered diazaborine binding affinity.[18]

Mutagenesis of Tyr158 and Lys165 in InhA Affects Triclosan Affinity

In contrast to the slow and tight binding observed between ecFabI and triclosan, triclosan is a rapid and reversible inhibitor of InhA. Triclosan binds to InhA in a similar way as triclosan binds to ecFabI; for example, Tyr158 and Lys165 of InhA have the same functional roles as the equivalent residues in ecFabI (Tyr156 and Lys163).[19] The residues involved in triclosan binding and resistance were mutated to see the differences in binding affinity and kinetics.[48,51] Tyr158Ser did not affect the activity of InhA, but Tyr158Phe and Tyr158Ala resulted in lower activity.[51] This finding suggested that Tyr158 is a critical residue that needs a hydroxyl group for proper function, which was verified using the Tyr158Phe mutation. This mutant also showed a decrease in triclosan binding affinity, verifying the requirement of a hydroxyl group at this position for efficient binding of triclosan.

Lys165 was mutated to Gln, Arg, Ala and Met to investigate the importance of the amine functional group in NAD binding. Gln and Arg substitutions did not affect the cofactor binding, while Ala and Met mutations abrogated cofactor binding, consistent with the proposed role of Lys165 in hydrogen bonding with the nicotinamide cofactor. Last, Met161Val and Ala124Val mutations were studied in InhA because these two mutations imparted triclosan resistance in *Mycobacterium smegmatis*.[52] The triclosan binding affinity was significantly lowered in both mutants of *M. tuberculosis* InhA.[48]

InhA has even been shown to bind two molecules of triclosan in the hydrophobic SBL of the active site (Figure 8).[52]

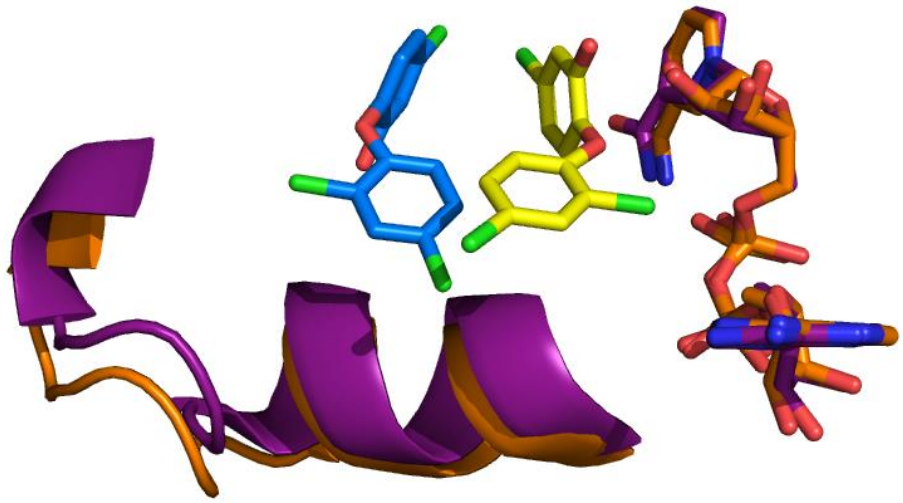

Figure 8: Structure of InhA and triclosan complex. The apo form of InhA (PDB ID: 1ENY) is shown in purple and the holo form of InhA with triclosan (PDB ID: 1P45) is shown in orange. NAD^+ is shown on the right with the two different colors correlating with their respective InhA forms. Triclosan1 is in blue and triclosan2 is in yellow.[53]

The difference in binding kinetics and strength observed between ecFabI and InhA appears to come from conformational differences in the SBL. Triclosan binding causes residues in the loop region of ecFabI to be more ordered, but for the triclosan binding in InhA, residues 197-211 in the SBL remain disordered.[47]

Conformational Change in SBLs of saFabI Occur Upon Triclosan Binding

Triclosan inhibits saFabI as a tight inhibitor, which is similar to the triclosan inhibition of ecFabI.[54] The main difference between saFabI compared to ecFabI and InhA is that saFabI uses NADPH or $NADP^+$ instead of the more commonly used NADH or NAD^+. This has been shown by the strong interaction of residues Arg40 and Lys41 in saFabI with the 2′-phosphate of NADPH.[54] Tyr157 and Lys164 of saFabI are the

structurally identical residues of Tyr156 and Lys163 of ecFabI and Tyr158 and Lys165 of InhA, which are the residues involved in binding of the substrate or inhibitor.[54] On top of the residues involved in the mechanism for reducing the double bond of the fatty acid substrate, other parts of the saFabI architecture play a critical role in substrate and inhibitor binding, such as the active site at residues 147 to 157 and two SBLs at residues 94 to 108 and residues 194 to 204 (Figure 9).[55]

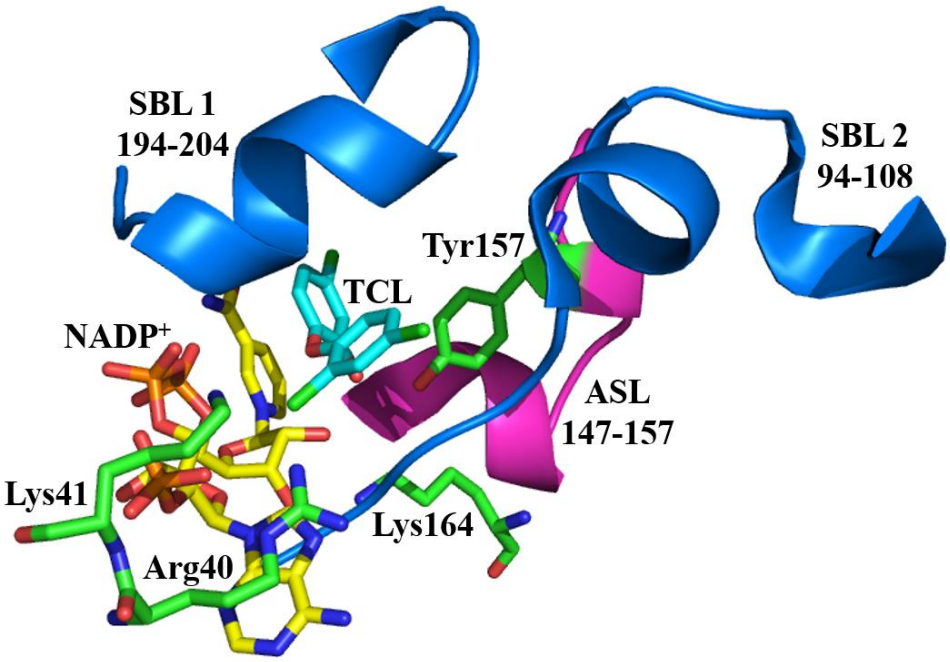

Figure 9: The active site and SBLs of abFabI. Triclosan (cyan) and NAD^+ (yellow) bound to abFabI with catalytic residues colored in green. The active site loop (residues 147-157) is colored in magenta and SBLs (residues 94-108 and 194-204) are colored in blue. Structure is from PDB ID: 4ALI.[55]

These regions are all disordered to begin with but become ordered upon inhibitor binding. The active site is open before binding of a cofactor and inhibitor. When an inhibitor such as triclosan binds, yielding the ternary complex, the SBLs closed over the active site. It is believed that residues Phe96 and Ser197 within the two SBLs trigger closing of the loops. Phe96 moves and allows for triclosan binding while Ser197 interacts with a water

molecule. This water molecule interacts with the carboxyl oxygen of a proximal Ala95 and causes Ala95 to undergo a conformational change that moves nearby residues and causes closure of the SBLs.

As described above with the other FabI homologs, mutations in the active site can confer antibiotic resistance. A missense mutation of Gly23Ser was suggested to make saFabI more resistant to triclosan.[17] Tyr147His, Phe204Cys, and Met99Thr are mutations that are also associated with increased triclosan resistance.[56] Further research on saFabI is required to fully understand triclosan resistance mechanisms.

Inhibition of InhA by Isoniazid

Before the 21st century, isoniazid was previously one of the leading drugs used to effectively treat *M. tuberculosis*. Isoniazid targets the InhA of *M. tuberculosis* with an IC_{50} value of 7.3 µM; the MIC value of isoniazid against *M. tuberculosis* is 5 µg/mL.[43] Unfortunately, *M. tuberculosis* is becoming resistant to isoniazid for reasons that are currently being investigated.[57] The current understanding about the mechanism of isoniazid is that the molecule is converted into a reactive form by a catalase-peroxidase called KatG before forming an adduct with NAD (Figure 10). This adduct inhibits InhA through a slow and tight binding mechanism similar to the diazaborine inhibition of ecFabI.[58]

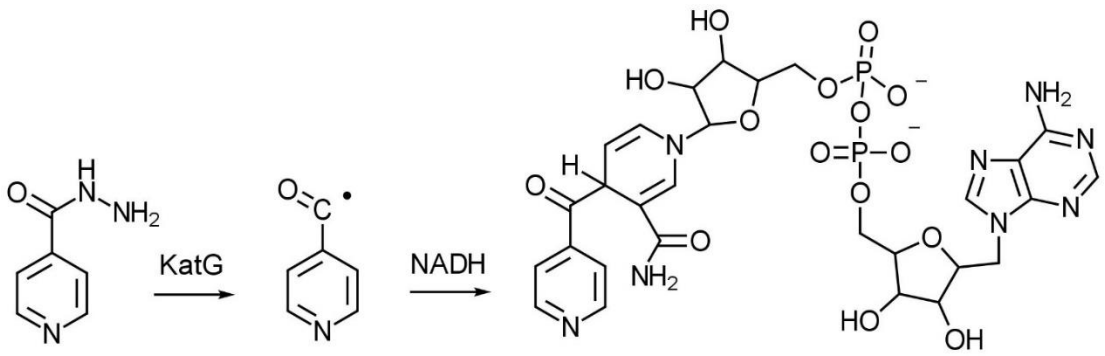

Figure 10: Formation of isoniazid-NAD by KatG activation.

Structural and steady state studies have shown that the isoniazid-NAD adduct is the actual InhA inhibitor and is formed even in the absence of InhA.[59,60] Comparisons were made with the structures to show that a conformational change occurs upon InhA binding the isoniazid-NAD adduct. The structures of InhA alone and InhA bound to NAD are the same, but in the structure of InhA bound to isoniazid-NAD, residues Phe149 and Met155 of InhA are shifted. Isoniazid-NAD binds in the same active site as NADH, so 50% of InhA is bound to NAD while the other 50% is bound to isoniazid-NAD. This finding hints at possible conformational changes that may also occur with FabI of other bacterial species upon inhibitor binding.

Besides understanding the mechanism of how isoniazid works on InhA, InhA has been regularly studied to reveal details on what specifically causes the evolving resistance. The mechanism of isoniazid inhibition was originally not well understood, so the early consensus on isoniazid resistance was based on mutations of InhA, specifically a natural missense mutation that led to Ser94Ala in InhA.[61] Many other natural mutations, especially of isoleucine residues such as Ile16Thr, Ile21Val, Ile47Thr, Ile95Pro, and Ile194Thr were proposed to be associated with isoniazid resistance. The aforementioned residues in wild-type InhA are proximal to NAD^+ (Figure 11).

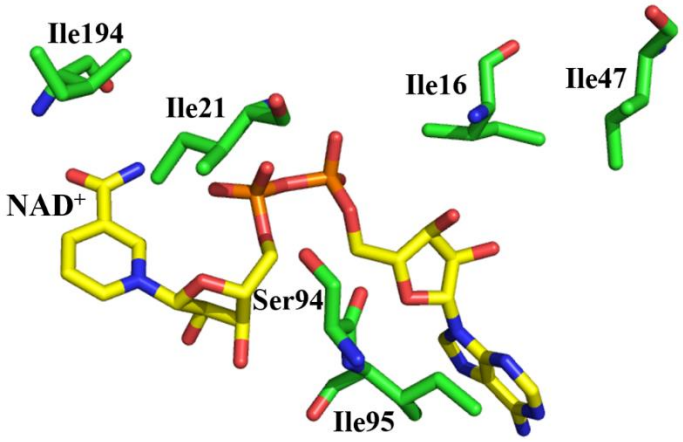

Figure 11: Residues of InhA that are involved in isoniazid resistance. The residues are shown in green and NAD^+ is shown in yellow.

Ile194Thr changes the specific pattern of binding between Ile194 and NADH, which causes a reduced binding affinity for NADH compared to the wild type InhA.[62] Ser94Ala (as mentioned above), Ile16Thr, Ile21Val, Ile47Thr, and Ile95Pro are all natural mutations from clinical isolates of isoniazid resistant InhA that show a decrease in binding affinity to NADH compared to wild type InhA. Ile95Pro has extremely poor binding to NADH and has the lowest binding affinity to NADH out of the four natural isoleucine mutations.[63] This study suggested a binding order of InhA binding to NADH to form a binary complex before isoniazid binds to the complex and inhibits InhA. Steady state kinetics in a later study were performed to support the model that isoniazid and NAD(H) form a binary complex before binding with InhA to form a ternary complex.[64] The mechanism of action for inhibition and the evolution of resistance in InhA and the FabI of other bacterial species continue to be under study.

Focus of the Current Project

Enoyl ACP Reductase of *Acinetobacter baumannii* (abFabI)

With the project at hand, the focus is to investigate the enoyl ACP reductase in a bacterial species called *Acinetobacter baumannii*, which is abbreviated abFabI. Since little is known about abFabI, we want to structurally and biochemically characterize the enzyme and work towards developing new drugs for inhibiting abFabI. At the start of the project, one of the objectives was to structurally characterize abFabI by X-ray crystallography. The enzyme's crystal structure has since been solved with NAD^+ by another research group (Figure 12).[30]

Figure 12: Crystal structure of abFabI. Structure is from PDB ID: 4ZJU. NAD^+ is shown in yellow sticks.

Having the solved crystal structure of abFabI as a guide can help with the structural comparison between abFabI and the enoyl ACP reductase from other bacterial

species. The sequence alignment of abFabI, ecFabI, InhA, and saFabI shows that many residues are conserved across species, but there are still a significant number of differences that narrow spectrum drugs can specifically target (Figure 13).[65]

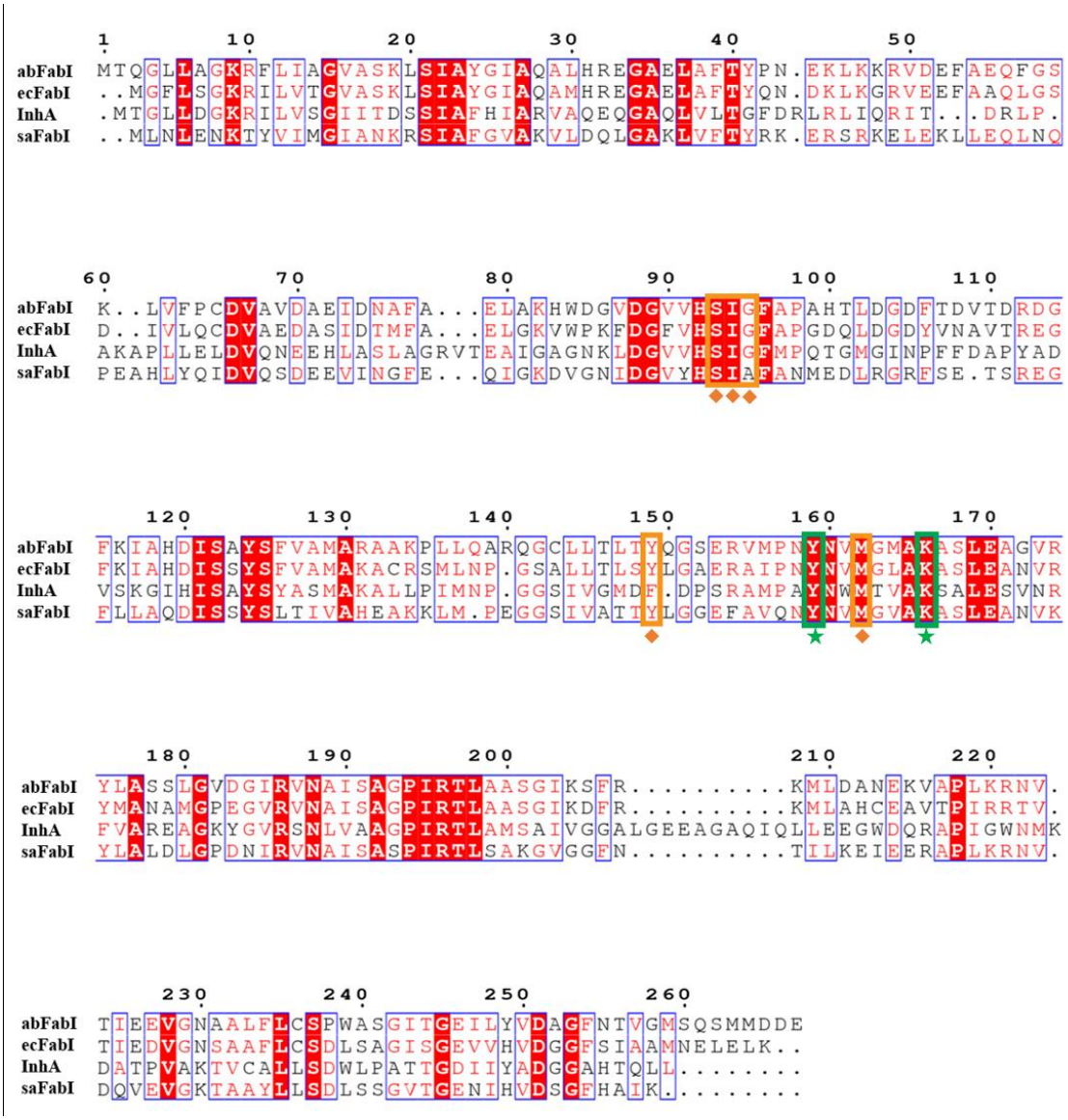

Figure 13: Sequence alignment of abFabI, ecFabI, InhA, and saFabI. Identical residues are highlighted in red. Similar residues are in red font and boxed in blue. The catalytic residues Tyr and Lys have been boxed in green with a star. The active residues are boxed in orange with a diamond.

The next step for us toward developing narrow-spectrum inhibitors against bacteria is to investigate potential abFabI inhibition by diazaborines, triclosan, and

isoniazid, including inhibition studies and solving structures of abFabI in complex with these known FabI inhibitors. The information generated from these studies can then be used to develop new drugs.

Rational Design of Novel Inhibitors Derived From Known FabI Inhibitors

The current research will determine if the diazaborines and triclosan can inhibit abFabI activity. Since diazaborines, isoniazid, and triclosan are becoming less efficacious, many research groups are rationally designing novel drugs or derivatives of the compounds. Many studies have shown lead compounds with higher activity than the previous drugs.[66-68] Inhibition studies can be used to enable drug development by structure-based design. These new therapeutics may also inhibit abFabI and be modified for use as a narrow spectrum drug for abFabI. This will remain unknown until more research has been done on abFabI and the inhibitors.

Research Goals

The enzyme abFabI is still not well understood. Even though FabI of other species have been highly studied, plenty of work has yet to be done on FabI specifically from *Acinetobacter baumannii*. The goal of the project is to enable drug development against *Acinetobacter baumannii* by examining the effect of several known FabI inhibitors on abFabI. My specific goals for the project is to 1) purify active abFabI, 2) perform inhibition studies using several known FabI inhibitors, and 3) solve the structure of abFabI with the inhibitors bound.

Methods Used to Study abFabI

Pure, soluble, and active abFabI is required for inhibition studies and structural characterization. Our approach includes protein expression in *E. coli*, purification of the protein, steady-state activity assays, and crystallization experiments. We used two main purification strategies: chromatographic separation methods applied to the soluble recombinant proteins expressed in *E. coli*, and denaturing preparations of the protein followed by chromatographic separations, applied to the insoluble recombinant proteins expressed in *E. coli*. The purification from inclusion bodies requires denaturation of abFabI by urea or guanidine hydrochloride followed by refolding of the protein by rapid dilution. Chromatographic methods used for purification of abFabI included nickel affinity chromatography, ion exchange chromatography, hydrophobic interaction chromatography, size exclusion chromatography, and Cibacron blue affinity chromatography. The activity of partially or fully purified protein samples was measured by enzyme activity assays in which NADH consumption was monitored at 340 nm. Purified protein was then used for crystallization experiments and for inhibition studies in which the IC_{50} of the known FabI inhibitor for abFabI was determined using our activity assay. The methods used to make, isolate, and assay abFabI resulted in pure and active protein that was used to show successful abFabI inhibition by three FabI inhibitors, which will be described in further detail in the next chapters.

Chapter 2

Materials and Methods

Materials

The abFabI gene was obtained in pET30 EK/LIC from Howard Xu, CSULA. Alternative expression vector pET-15b was obtained from EMD Millipore, Inc., and pBG100 and pBG106 (both of which are pET27 derivatives) were from Vanderbilt University's Center for Structural Biology. Double digestion reagents were purchased from Thermo Fisher Scientific. T100 Thermal Cycler and DNA and protein electrophoresis materials were from Bio-Rad Laboratories. The program QuantityOne for a BioRad ChemiDoc XRS gel imaging system of a Universal Hood II was used to document DNA and protein gels. Centrifugation steps were carried out using a Sorvall Legend Micro 21R Centrifuge, a Sorvall Legend X1R Centrifuge, or a Beckman Coulter Avanti J-E Centrifuge (JA-20). ÄKTA PrimePlus Fast Protein Liquid Chromatography (FPLC) and chromatography columns were purchased from GE Healthcare. UV-Vis absorption measurements and spectra were collected using an Agilent Cary 60 UV-Vis Spectrophotometer.

Analysis of the abFabI DNA and Protein Sequences

The abFabI DNA sequence was confirmed by sequencing (Laragen, Inc) to verify that no mutations were present. Our abFabI protein sequence (Figure 14), which is referred to abFabI-1, was analyzed by the BLAST tool in the Uniprot database for the identification of homologs and also the structure analysis tools available through the ExPASy server (https://www.expasy.org/structural_bioinformatics) such as Protein

Model Portal for structural information for a protein and SWISS-MODEL for protein structure homology.

MHHHHHHSSGLVPRGSGMKETAAAKFERQHMDSPDLGTDDDDKMQFRKTLNI
GIMLKIVLSEIGMTQGLLAGKRFLIAGVASKLSIAYGIAQALHREGAELAFTYPNE
KLKKRVDEFAEQFGSKLVFPCDVAVDAEIDNAFAELAKHWDGVDGVVHSIGFA
PAHTLDGDFTEVTDRDGFKIAHDISAYSFVAMARAAKPLLQARQGCLLTLTYQG
SERVMPNYNVMGMAKASLEAGVRYLASSLGVDGIRVNAISAGPIRTLAASGIKS
FRKMLDANEKVAPLKRNVTIEEVGNAALFLCSPWASGITGEILYVDAGFNTVGM
SQSMMDDE.

Figure 14: Protein sequence of abFabI-1.

Subcloning abFabI into Plasmids

Two versions of the abFabI gene were subcloned from the pET30 EK/LIC plasmid (pAbFabI-1), which includes abFabI-1, into three unique expression vectors (Table 6). The more common, shorter gene is referred to as abFabI-a, and the longer N-terminally extended version is referred to as abFabI-b. See Chapter 3 for information on the two versions of abFabI investigated here.

Vector	Provider	N-terminal Tag	Cleavage Site	Resistance Marker
pET-15b	EMD Millipore, Inc.	6xHis-tag	Thrombin	Ampicillin
pBG100	Vanderbilt University	6xHis-tag	HRV 3C (PreScission)	Kanamycin
pBG106	Vanderbilt University	10xHis-tag	HRV 3C (PreScission)	Kanamycin

Table 6: Plasmids used for subcloning.

The abFabI gene was amplified from pET30 EK/LIC using primers with specific restriction sites designed into the 5′ and 3′ ends to facilitate subcloning. Seven total expression constructs were generated (pAbFabI-1 and two versions of abFabI cloned into each of the three vectors listed in Table 6), but only pAbFabI-1 and pET-15b plasmids pAbFabI-2a and pAbFabI-2b (Figure 15) were later used in expression trials.

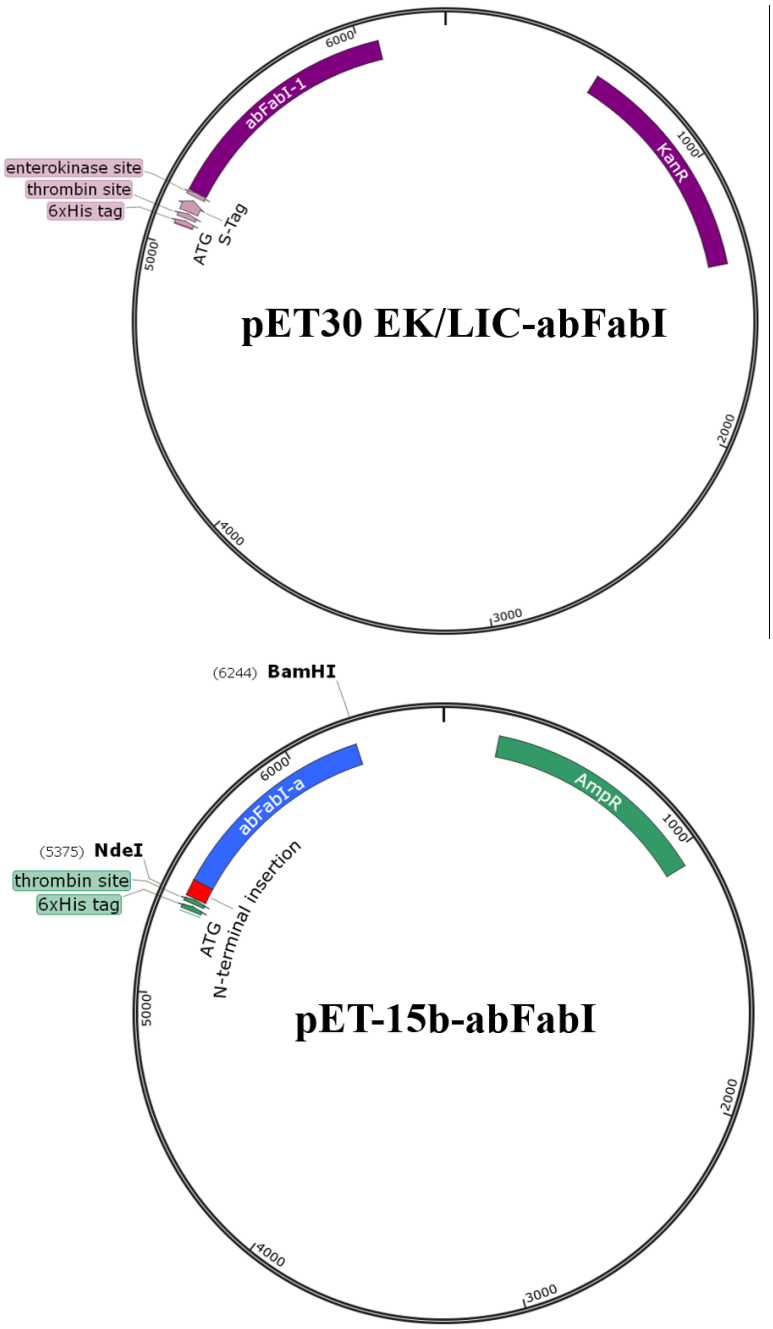

Figure 15: Plasmids pET30 EK/LIC and pET-15b contain the abFabI gene. Top: pET30 EK/LIC contains the abFabI-1 construct and kanamycin resistance marker. Bottom: The subcloning process uses restriction sites to insert the abFabI gene. Both versions of abFabI were separately inserted into pET-15b expression vectors. The shorter version (abFabI-a) is in blue and the N-terminal insertion is in red. The longer version (abFabI-b) is illustrated in this image; the abFabI-b is identical to this factor, with the exception of the N-terminal insertion. pET-15b plasmids contain the ampicillin resistance marker.

Polymerase Chain Reaction

Primers were purchased from Life Technologies Corporation (Table 7).

Plasmid	Protein	Primer Sequence	Restriction Enzyme
pAbFabI-2a	abFabI-2a	Forward: GACCATATGACACAAGGACTTTTAG Reverse: CGAACTGGATCCTTATTCATCATC	5′ end: NdeI 3′ end: BamHI
pAbFabI-2b	abFabI-2b	Forward: GACATTCATATGCAATTTCGAAAA Reverse: CGAACTGGATCCTTATTCATCATC	5′ end: NdeI 3′ end: BamHI
pAbFabI-3a	abFabI-3a	Forward: GACGGATCCATGACACAAGGACTTTTAG Reverse: CGAACTCTCGAGTTATTCATCATC	5′ end: BamHI 3′ end: XhoI
pAbFabI-3b	abFabI-3b	Forward: GACATTGGATCCATGCAATTTCGA Reverse: CGAACTCTCGAGTTATTCATCATC	5′ end: BamHI 3′ end: XhoI
pAbFabI-4a	abFabI-4a	Forward: GACGGATCCATGACACAAGGACTTTTAG Reverse: CGAACTCTCGAGTTATTCATCATC	5′ end: BamHI 3′ end: XhoI
pAbFabI-4b	abFabI-4b	Forward: GACATTGGATCCATGCAATTTCGA Reverse: CGAACTCTCGAGTTATTCATCATC	5′ end: BamHI 3′ end: XhoI

Table 7: Primer information used for PCR. The sequence recognized by the restriction enzyme is underlined for each primer.

Each insert sequence was amplified by PCR using reaction mixtures consisting of 1X Phusion HF buffer, 0.5 µM forward primer, 0.5 µM reverse primer, 0.5 µM template DNA, 200 µM dNTPs, 2% DMSO, 1 mM $MgCl_2$, and 1 U of Phusion Hot Start II DNA polymerase (1 U = amount of enzyme that will incorporate 10 nmoles of dNTPs into a polynucleotide fraction at 74°C in 30 min). This sample amplified in a BioRad thermal cycler using a protocol that denatured the DNA oligonucleotides at 98°C for 30 seconds and then carried out 30 cycles of denaturation at 98°C for 10 seconds, annealing at 62°C for 30 seconds, and elongation at 72°C for 3 minutes 9 seconds. A final elongation step at 72°C for 10 minutes was completed before allowing the sample to incubate at 4°C.

Agarose Gel Electrophoresis

The amplified PCR products were purified by agarose gel electrophoresis. A 1% agarose gel was made by mixing 0.5 g of agarose with 50 mL of 0.5X TBE buffer (45 nM Tris, 45 nM boric acid, 0.8 mM EDTA, pH 8.3). 0.5 µL SYBRSafe (Thermo Fisher), a

safer alternative than the conventional ethidium bromide, was added to dissolved agarose for visualizing the DNA bands under UV light after completion of the gel electrophoresis. The samples were run on the gel at 100 mV for 1 hour in 0.5X TBE buffer.

Gel Extraction

The PCR products were excised from the DNA gel and purified at room temperature using the GeneJET Gel Extraction Kit (Thermo Scientific). Binding buffer was added to the weighed gel slice at a 1:1 w/v ratio before dissolving the contents at 55^{o}C for 10 minutes. The solution was then transferred to a GeneJET purification column and centrifuged. Wash buffer with ethanol was added to the column and then centrifuged. The purified DNA sample was eluted with water and stored at -20^{o}C.

Double Digestion

Each target plasmid and the PCR-amplified insert sequences were double digested in preparation for ligation. The restriction enzymes NdeI and BamHI were used on the insert sequence and target plasmid of pET-15b (pAbFabI-2a and -2b). Another pair of restriction enzymes, BamHI and XhoI, was used to digest the insert sequence and target plasmids of pBG100 (pAbFabI-3a and -3b) and pBG106 (pAbFabI-4a and -4b). A 50 µL reaction mixture was prepared for the various double digestion products (Table 8). The double digested products were purified using an agarose gel and extracted using the GeneJET Gel Extraction Kit.

pET-15b insert	pET-15b plasmid	pBG100/pBG106 insert	pBG100/pBG106 plasmid
28 µL dH_2O 10 µL 2X Tango buffer 10 µL PCR product 1 µL NdeI 1 µL BamHI	27 µL dH_2O 10 µL 2X Tango buffer 10 µL target plasmid 1 µL NdeI 1 µL BamHI 1 µL alkaline phosphatase	28.5 µL dH_2O 10 µL 2X Tango buffer 10 µL PCR product 1 µL BamHI 0.5 µL XhoI	27.5 µL dH_2O 10 µL 2X Tango buffer 10 µL target plasmid 1 µL BamHI 0.5 µL XhoI 1 µL alkaline phosphatase

Table 8: Ingredients and volumes for double digestion products.

Ligation

The purified digestion products were ligated using T4 DNA ligase. Each 10 µL reaction mixture contained 6 µL digested insert sequence, 2 µL digested target plasmid (3:1 ratio of insert to target plasmid), 1 µL T4 DNA ligase, and 1 µL T4 DNA ligase reaction buffer. This reaction mixture was allowed to incubate at 4^{o}C overnight.

E. coli Transformation by Heat Shock

The ligated plasmids were transformed into *E. coli* (DH5α) cells. *E. coli* (DH5a) competent cells were used for DNA amplification and BL21 (DE3) competent cells were used for expression purposes. The competent cells were mixed and incubated with plasmid at 0^{o}C for 30 minutes and heat shocked at 37^{o}C for 5 minutes, followed by a brief recovery at 0^{o}C for 2 minutes. LB media was added to the cells and incubated at 37^{o}C for 1 hour to allow synthesis of the antibiotic resistance marker and then selected on LB-agarose plates with the appropriate antibiotic (Table 9). The plates were incubated at 37^{o}C for 12 to 16 hours to allow the successfully transformed cells to form colonies and stored at 4^{o}C.

Expression Vector	Antibiotic Resistance
pET30 EK/LIC	Kanamycin
pET-15b	Ampicillin
pBG100	Kanamycin
pBG106	Ampicillin

Table 9: Expression vectors and their antibiotic resistance.

Confirmation of Successful Subcloning

Colonies on each post-ligation plate were grown in 5 mL LB cultures with the appropriate antibiotic for 12 to 16 hours at 37^{o}C. Cells were harvested by centrifugation, and the plasmid DNA in those cells was purified using the GeneJET Plasmid Miniprep Kit (Thermo Scientific). Resuspension solution with RNase A, lysis solution, and neutralization solution were sequentially added to the cells and centrifuged for 5 minutes to separate the cell debris from the plasmid DNA. The supernatant that includes the plasmid DNA was transferred to a GeneJET spin column and centrifuged for 1 minute. Wash solution that included ethanol was added to the column and centrifuged for 1 minute for a total of three times. Finally, water was added, incubated for 2 minutes at room temperature, and centrifuged for 2 minutes to elute the plasmid DNA. The plasmid DNA was stored at -20^{o}C and sequenced by Laragen, Inc.

Expression of abFabI of Different Vectors in *E. coli* Cells

A colony on a plate was grown in 5 mL of LB culture with the appropriate antibiotic for 12 to 16 hours at 37^{o}C. 1 mL of LB culture was added to 1 L of LB media. After allowing the 1 L of cells in LB medium to reach an optical density at 600 nm (OD_{600}) of 0.600 absorbance units, isopropyl β-D-1-thiogalactopyranoside (IPTG) was added to a final concentration of 1 mM to begin protein induction.

Cultures were incubated at 18^{o}C for 18 hours after induction of protein expression. The cell pellets were harvested by centrifugation at 5,000 rpm for 15 minutes, suspended in 5 mL lysis buffer (50 mM Tris-Cl and 500 mM NaCl at pH 8.5) per gram of cells, and stored at -20^{o}C for future use. Samples before and after protein induction were collected for sodium dodecyl sulfate polyacrylamide gel electrophoresis (SDS-PAGE). 1 mL of the culture was collected and the cell pellet was separated from the supernatant by centrifuging at 5,000 rpm for 5 minutes. The volume of loading buffer was calculated to normalize the protein concentration for SDS-PAGE (Equation 1).

$$\mu L \text{ loading buffer} = [(OD_{600} \text{ of culture})/0.600] \times (V_{\text{cell culture sample}} \text{ in mL} \div 10) \times 1000$$

Equation 1: Calculation for volume of loading buffer.

SDS-PAGE and Native PAGE

SDS-PAGE (visualizes denatured monomers) and Native PAGE (visualizes oligomeric state) were performed to separate proteins by molecular weight. Gels were made with a 12% separating layer that consisted of 30% acrylamide/bisacrylamide solution, 4X Tris/SDS at pH 8.8, 10% ammonium persulfate, and tetramethylethylenediamine (TEMED), and a stacking layer that consisted of 30% acrylamide/bisacrylamide solution, 4X Tris/SDS at pH 6.8, 10% ammonium persulfate, and TEMED. Samples were loaded on the gels and electrophoresed in a 25 mM Tris, 192 mM glycine, 0.1% (w/v) SDS, pH 8.3 buffer at 100 mV for 10 minutes. The gels were then electrophoresed at 130 mV for 75 minutes to separate and view the proteins. A buffer that contained 50% methanol, 40% water, 10% acetic acid, and 0.05% (w/v) Brilliant Blue was used for staining, and a buffer containing 80% water, 10% methanol,

and 10% acetic acid was used for destaining. Native PAGE gels were made and performed in the same way as SDS-PAGE gels with the exception that SDS was omitted from all solutions.

Protein Purification Methods

Cell Lysis

Cell pellets that were frozen in lysis buffer were thawed and kept on ice throughout the purification process. The following reagents were added to the cell culture suspension prior to sonication: lysozyme (final concentration 0.25 mg/mL), PMSF (1 mM), DNase (10 µg/mL), and RNase (10 µg/mL). Sonication of the cells was performed at 50% amplitude in 5 second intervals with a Fisher Scientific Ultrasonic Processor. Cells were sonicated for 18 cycles for a total of 3 minutes to reach a translucent state. The supernatant (soluble) and pellet (insoluble) were separated by centrifugation at 20,000 rpm for 30 minutes at 4^{o}C. Samples of both portions were collected for SDS-PAGE.

Purification from Supernatant

The supernatant from the lysed cells was filtered with a 0.45 µm filter and loaded into a superloop. An ÄKTA PrimePlus FPLC was used to purify abFabI by nickel affinity chromatography (HisPrep^{TM} FF 16/10), size exclusion chromatography (HiPrep^{TM} 26/60 Sephacryl^{TM} S-300 HR), cation exchange chromatography (HiPrep^{TM} SP XL 16/10), anion exchange chromatography (HiPrep^{TM} Q XL 16/10), hydrophobic interaction chromatography (HiPrep^{TM} Phenyl FF (low sub) 16/10), or Cibacron blue affinity

chromatography (HiPrep^{TM} Blue HP). See Table 10 and 11b for descriptions of the binding and elution buffers used for each column type. Protein elution was monitored using a UV detector set to 280 nm. Fractions containing protein (corresponding to peaks in the absorbance at 280 nm) were collected and electrophoresed on an SDS-PAGE gel. Any fractions that included abFabI were concentrated and dialyzed in a buffer of 50 mM Tris-Cl at pH 8.5 for use in future experiments.

Chromatography Type	Binding Buffer	Elution Buffer
Nickel Affinity	50 mM Tris-Cl 150 mM NaCl pH 7.5	50 mM Tris-Cl 150 mM NaCl 500 mM Imidazole pH 7.5
Size Exclusion	50 mM Tris-Cl 150 mM NaCl pH 7.5	50 mM Tris-Cl 150 mM NaCl pH 7.5
Cation Exchange	50 mM $NaCH_3COO$ pH 5.5	50 mM $NaCH_3COO$ 1 M NaCl pH 5.5
Anion Exchange	20 mM Tris-Cl pH 8.0	20 mM Tris-Cl 1 M NaCl pH 8.0
Hydrophobic Interaction	50 mM NaH_2PO_4 1.5 M $(NH_4)_2SO_4$ pH 7.0	50 mM NaH_2PO_4 pH 7.0

Table 10: Buffers used to purify abFabI from supernatant.

Purification from Inclusion Bodies

The cell break pellet (the insoluble cell debris remaining after cell lysis, which includes inclusion bodies) was used for purification and refolding of misfolded abFabI. Inclusion bodies in the cell break pellet were washed to remove contaminants, especially proteases, by resuspension in wash buffer (Table 11a), sonication, and centrifugation at 20,000 rpm for 15 minutes at 4^{o}C. Rapid dilution was performed by denaturing the pellet in solubilization buffer (Table 11a), sonicating for 1 minute at 50% amplitude for

5 second intervals to ensure the denatured protein was homogenous, and refolding the protein by dilution. The protein was diluted slowly (drop by drop) into a large volume of refolding buffer (Buffer 12 of AthenaES QuickFold™ Protein Refolding Kit) to allow individual proteins to fold in isolation. In a typical refolding experiment, 1 mL denatured protein was diluted into 20 mL of refolding buffer (Table 11a) and allowed to refold for 1 hour at 4°C. The refolded protein was concentrated and dialyzed into an appropriate buffer (Table 11b) in preparation for further chromatographic purification.

a)

Wash Buffer	Solubilization Buffer	Refolding Buffer
50 mM Tris-Cl 500 mM NaCl 1 mM EDTA pH 8.5	50 mM Tris-Cl 8 M urea 10 mM β-mercaptoethanol pH 8.5	50 mM Tris-Cl 240 mM NaCl 10 mM KCl 1 mM EDTA 0.05% PEG 3350 1 mM GSH 1 mM GSSH pH 8.5

b)

Chromatography Type	Binding Buffer	Elution Buffer
Nickel Affinity	50 mM Tris-Cl 150 mM NaCl pH 7.5	50 mM Tris-Cl 150 mM NaCl 500 mM Imidazole pH 7.5
Size Exclusion	50 mM Tris-Cl 150 mM NaCl pH 7.5	50 mM Tris-Cl 150 mM NaCl pH 7.5
Cation Exchange	50 mM $NaCH_3COO$ pH 5.5	50 mM $NaCH_3COO$ 1 M NaCl pH 5.5
Anion Exchange	20 mM Tris-Cl pH 8.0	20 mM Tris-Cl 1 M NaCl pH 8.0
Hydrophobic Interaction	50 mM NaH_2PO_4 1.5 M $(NH_4)_2SO_4$ pH 7.0	50 mM NaH_2PO_4 pH 7.0
Cibacron blue Affinity	50 mM Tris-Cl pH 8.5	50 mM Tris-Cl 10 mM NADH pH 8.5

Table 11: Buffers used to purify abFabI from inclusion bodies.

Protein Band Identification by Sequence Analysis

Selected protein bands on our SDS-PAGE gels were identified by mass spectrometry. Bands were excised from the gels and submitted for sequencing at the UCLA *Molecular Instrumentation Center*. Databases and tools on ExPASy (www.expasy.org/proteomics/post-translational_modification), like GPS for phosphorylation sites, GPS-SUMO for sumoylation sites, and SwissPalm for palmitoylation, were utilized to analyze the abFabI sequence potential protein modification sites.

NADH Consumption Assay

Enzyme activity was determined using an NADH consumption assay in which NADH disappearance was monitored in a 1 cm pathlength cuvette at 340 nm on an Agilent Cary 60 UV-Vis spectrophotometer using the Kinetics application.[69] The specific activity of the protein was calculated as shown in Equation 2.

$$\text{Specific activity} = \frac{[(\text{NADH consumption rate/min})/6220\ M^{-1}cm^{-1}] \bullet 10^6\ \mu M/M \bullet 1\ cm}{\text{mg of abFabI used in assay}}$$

Equation 2: Calculation for specific activity of abFabI. The specific activity is in μM/min·mg and the NADH consumption rate is in absorbance units/min. 6220 $M^{-1}cm^{-1}$ is the NADH extinction coefficient at 340 nm.

Reaction mixtures consisted of 150 mM NaCl, 20 mM Tris-Cl at pH 8.5, 0.5 μM abFabI, 200 μM crotonyl-CoA, and 100 μM NADH in 100 μL total volume. Crotonyl-CoA, the substrate used in the assay, is an analog of a FAS-II pathway substrate crotonyl-ACP. All reagents were mixed together excluding NADH. The mixture without NADH was

blanked prior to adding NADH to initiate the reaction. Initial reaction rates were obtained by allowing the reactions to run for 1 minute.

Inhibition Assay

Percent inhibition by each inhibitor was determined by carrying out a standard activity assay in the presence of an inhibitor. Activity was monitored in a 1 cm pathlength cuvette at 340 nm with an Agilent Cary 60 UV-Vis spectrophotometer using the Kinetics application. The 100 µL inhibition assay mixture contained 150 mM NaCl, 20 mM Tris-Cl at pH 8.5, 0.5 µM abFabI, 100 µM NAD^+, 200 µM crotonyl-CoA, and 100 µM NADH. Inhibitors triclosan, isoniazid, and diazaborines 14b, 18c, 35b, and 39 (from Dr. Michael Groziak, CSU East Bay) were dissolved in 100% DMSO and were diluted to a final concentration of 2.9% DMSO in the 100 µL mixture. The control experiments included 2.9% DMSO with no inhibitor. Various concentrations of inhibitors were included in the assays and all reagents besides NADH were mixed together and blanked. The mixture was then incubated for 10 minutes at room temperature to allow for the abFabI:inhibitor:NAD^+ complex to form before adding NADH to begin the reaction. Initial reaction rates were obtained by allowing the reactions to run for 1 minute. IC_{50} plots were generated and fitted using the KaleidaGraph software package.

Chapter 3

Results and Discussion

The abFabI-1 Sequence in the pAbFabI-1 Vector

The pAbFabI-1 vector (a derivative of pET30 EK/LIC) was obtained from Dr. Howard Xu at CSULA. The pET30 EK/LIC expression vector confers two tags to the N-terminus of a gene inserted at its cloning site: an S-tag for improving protein solubility and a 6xHis tag for purification by nickel affinity chromatography. Our abFabI-1 expression construct had a leucine to tryptophan point mutation at position 7 that needed correction, so a Trp7Leu mutation was performed (Mike Serobyan, CSUN). The DNA sequence of the corrected abFabI-1 was confirmed by DNA sequencing, showing successful point mutation to the correct abFabI sequence. The protein sequence of abFabI-1 is shown below (Figure 16) with the N-terminal features that were conferred by the plasmid shown in bold (blue text corresponds to the 6-His tag, magenta text is the thrombin cleavage site, orange text is the S-tag, and green text is the enterokinase cleavage site). The abFabI gene sequence-based N-terminal insertion (see section **Discussion of the N-terminal Insertion in abFabI-b)** is shown in red text. The point mutation that was corrected by Mike Serobyan is underlined.

MHHHHHHSSGLVPRGSGMKETAAAKFERQHMDSPDLGTDDDDKMQFRKT
LNIGIMLKIVLSEIGMTQGLLAGKRFLIAGVASKLSIAYGIAQALHREGAELAFTY
PNEKLKKRVDEFAEQFGSKLVFPCDVAVDAEIDNAFAELAKHWDGVDGVVHSI
GFAPAHTLDGDFTEVTDRDGFKIAHDISAYSFVAMARAAKPLLQARQGCLLTLT
YQGSERVMPNYNVMGMAKASLEAGVRYLASSLGVDGIRVNAISAGPIRTLAAS
GIKSFRKMLDANEKVAPLKRNVTIEEVGNAALFLCSPWASGITGEILYVDAGFNT
VGMSQSMMDDE.

Figure 16: Protein sequence of abFabI-1.

Expression of abFabI-1

Expression trials were carried out to determine the best protein expression conditions for abFabI-1 in *E. coli* BL21 (DE3) cells. Induction temperature, induction time, and IPTG concentration were adjusted to optimize abFabI expression with the goal of finding conditions that would provide high amounts of soluble protein. Incubation temperatures of 18ºC, 25ºC, and 37ºC with incubation times ranging from 1 hour to 24 hours were tested, and protein expression was induced with IPTG concentrations of either 0.5 mM or 1.0 mM (Figure 17).

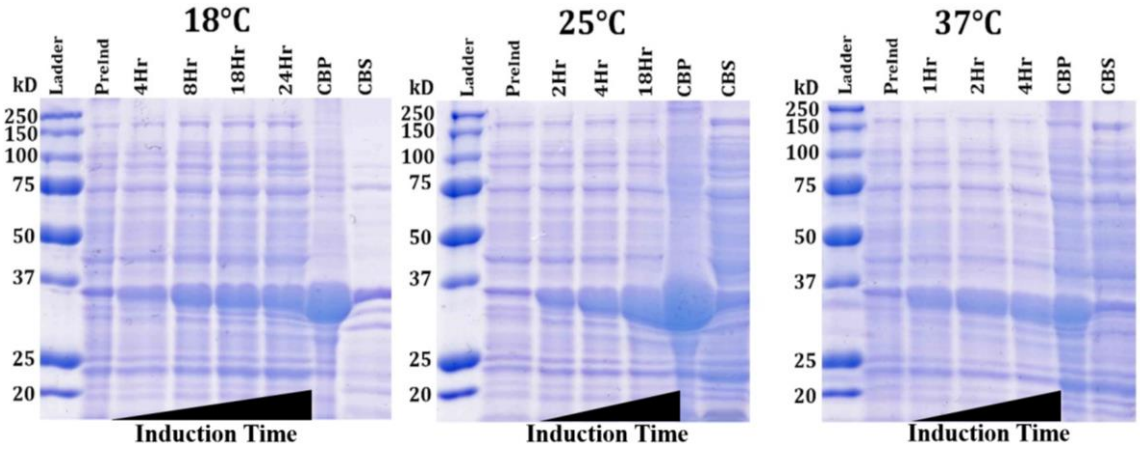

Figure 17: Expression trials of abFabI-1. These SDS-PAGE gels show the protein content of cell culture samples taken before and during protein expression with 1.0 mM IPTG used to induce expression. The timepoints at which each culture was sampled are indicated on the figure. The pellet (CBP) or supernatant (CBS) obtained after lysis of a small sample of harvested cells is included to indicate protein solubility. The predicted molecular weight abFabI-1 is 35.8 kDa.

A large amount of protein at 35.8 kDa is seen in the cell break pellet (CBP) while a very small amount of protein is in the cell break supernatant (CBS). abFabI-1 appears to be primarily misfolded in the CBP at the induction temperatures tested, but there is still folded soluble protein in the CBS of each temperature. Comparing the intensity of the

presumed abFabI-1 band with those of the native *E. coli* proteins, it looks like 18^{o}C yields the most soluble abFabI-1.

Protein Purification from the Soluble Cell Portion

abFabI-1 expressing cells that were induced and incubated at 18^{o}C for 18 hours were lysed by sonication and centrifuged to isolate soluble proteins. The soluble proteins were fractionated using five chromatography types in order to assess each column's effectiveness in yielding pure abFabI. Nickel affinity, size exclusion, cation exchange, anion exchange, and hydrophobic interaction chromatography (HIC) were used, with HIC being the most successful of the five. Chromatographic separations were assessed using SDS-PAGE to visualize protein purity levels, and activity assays were employed to quantitate the amount of active abFabI-1 present. These initial experiments to optimize our purification methods were carried out on small scales (using maximum culture volumes of 1 L to test each column type).

Protein Separation by Nickel Affinity Chromatography

Because abFabI-1 has an N-terminal 6xHis tag, we first used nickel affinity chromatography to purify it. In theory, the native *E. coli* proteins do not bind the nickel nitrilotriacetic acid (Ni-NTA) resin while abFabI-1 binds Ni-NTA via the 6xHis tag and is later eluted by an imidazole wash. Contrary to our expectations, purification from the CBS resulted in abFabI-1 not binding to the Ni-NTA column and appearing in the flow through (Figure 18).

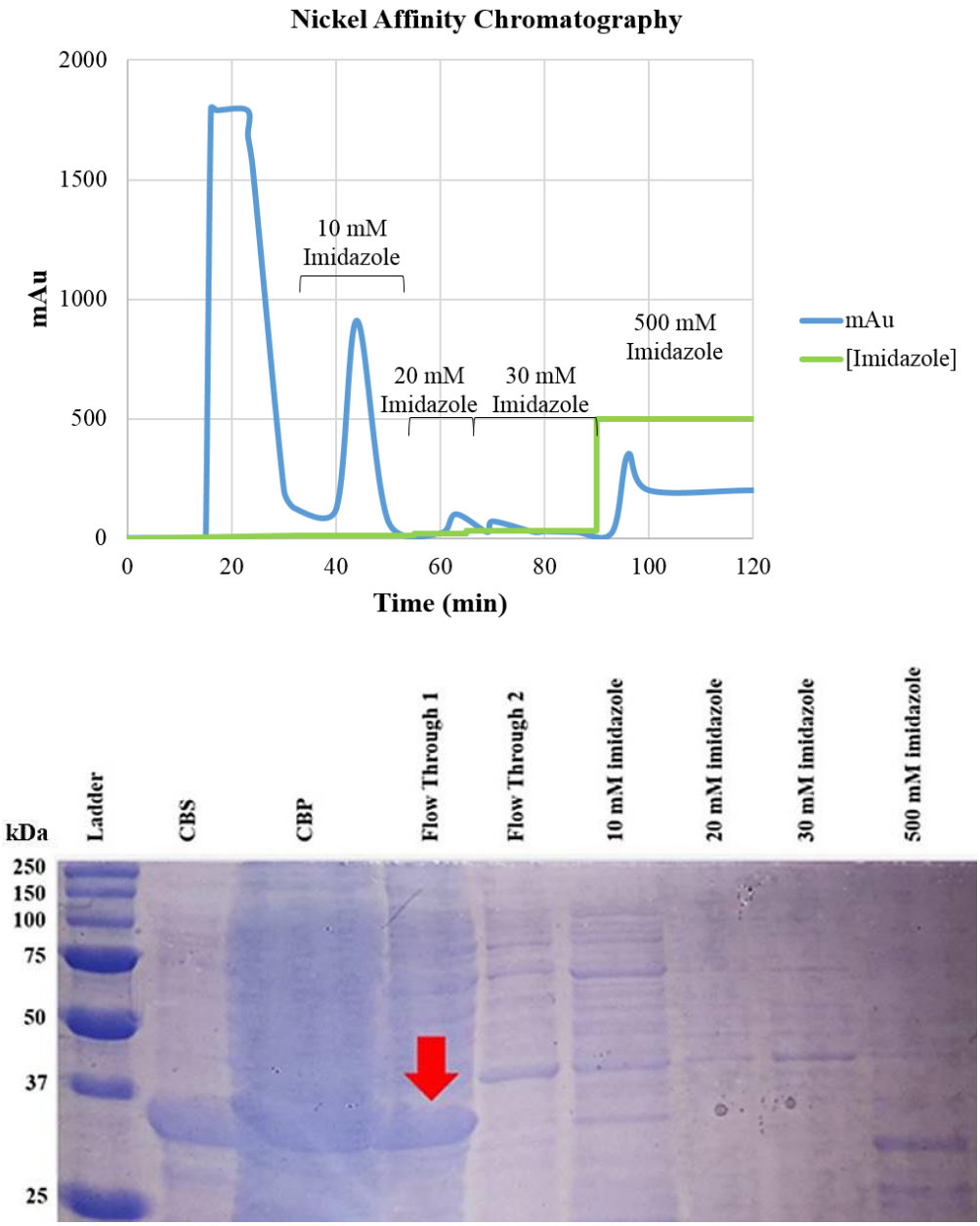

Figure 18: SDS-PAGE gel and UV trace of nickel affinity chromatography. The blue line is mAu at 280 nm and the green line is the imidazole concentration in mM. Peaks correspond to 1) flow through and 2) 10 mM, 3) 20 mM, 4) 30 mM, and 5) 500 mM imidazole elution.

Washes of 10-500 mM imidazole did not yield any pure abFabI-1 since abFabI-1 did not bind to the Ni-NTA. The 6xHis tag may possibly be occluded, which may account for the protein of interest not binding to the Ni-NTA resin. Since the 6xHis tag needs to be

exposed in order to bind to the resin, the occlusion could be due to the 6xHis tag being buried by other amino acids in the protein sequence.

Protein Separation by Size Exclusion Chromatography

Size exclusion chromatography was used in an attempt to purify abFabI-1, but no protein was collected (Figure 19) since the maximum peak was only 150 mAu.

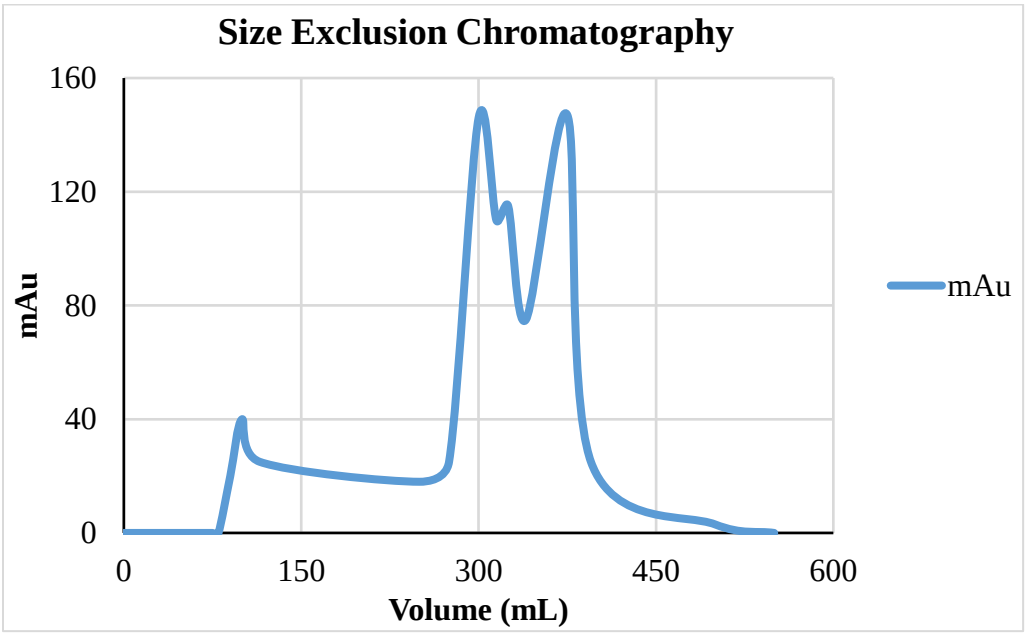

Figure 19: UV trace of size exclusion chromatography. The blue line represents mAu at 280 nm.

The sample was too dilute, so not enough protein was even recovered to perform any further experiments. A higher protein concentration is needed in order to use the size exchange chromatography for purification.

Protein Separation by Ion Exchange Chromatography

Ion exchange chromatography was used to try to separate abFabI-1 from other proteins by exploiting differences in the overall charge of the proteins in the sample. The isoelectric point (pI) of abFabI-1 is 6.08; therefore, at pHs lower than 6.08, the protein will be positively charged and at pHs higher than 6.08, the protein will be negatively charged. The overall charge on the protein can be controlled and manipulated to achieve protein separation by altering the pH of the buffer. Cation exchange chromatography (HiPrep™ SP XL 16/10) at pH 5.5 (Figure 20) and anion exchange chromatography (HiPrep™ Q XL 16/10) at pH 9 (Figure 21) were performed separately with the CBS. The protein did not bind to either column and eluted in the flow through.

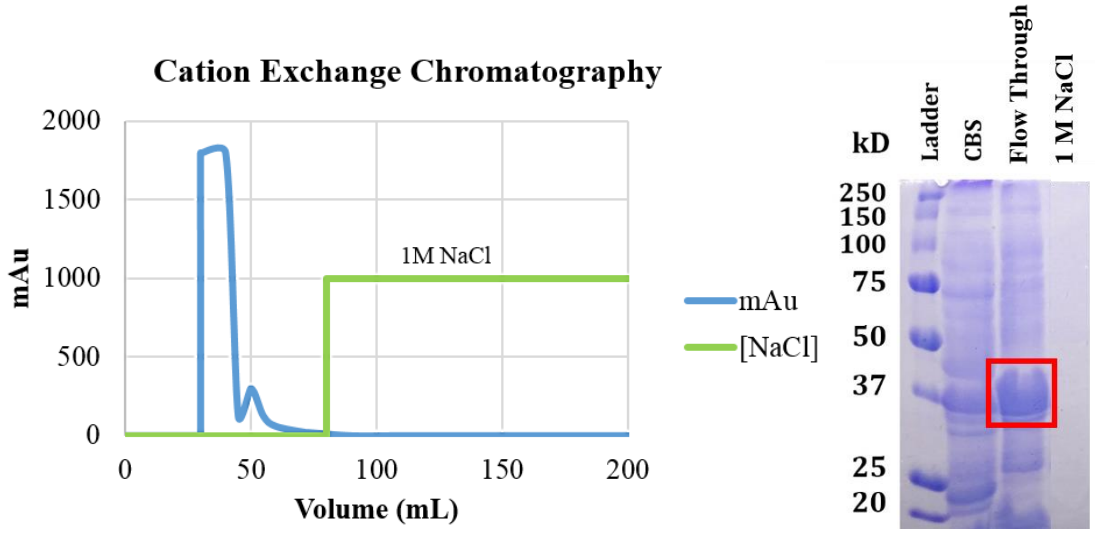

Figure 20: SDS-PAGE gel and UV trace for cation exchange chromatography. SDS-PAGE gel and UV trace for cation exchange chromatography. The band corresponding to abFabI-1 is boxed in red in the SDS-PAGE gel. The blue line is mAu at 280 nm and the green line is the sodium chloride concentration in mM.

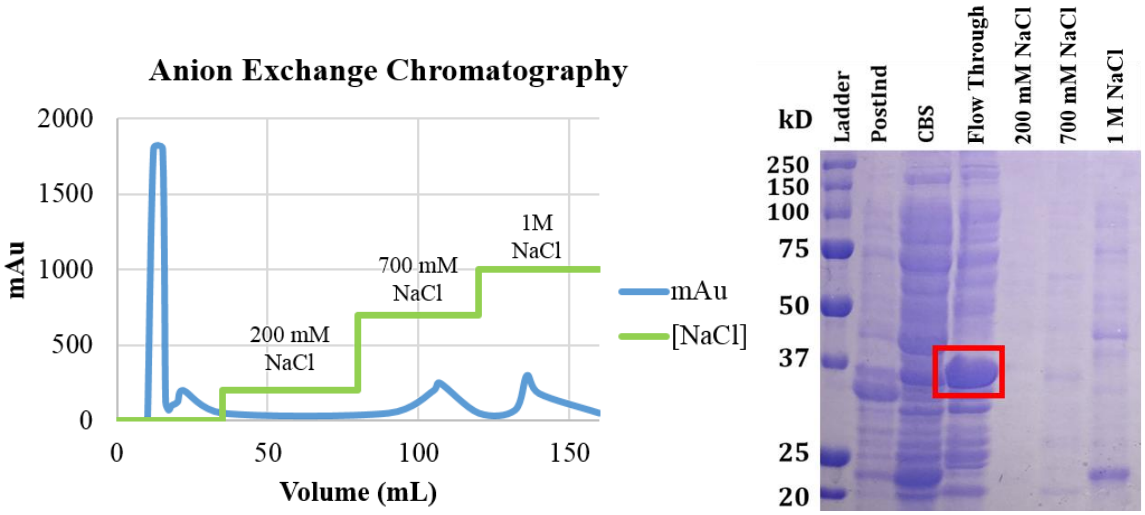

Figure 21: SDS-PAGE gel and UV trace for anion exchange chromatography. SDS-PAGE gel and UV trace for anion exchange chromatography. The band corresponding to abFabI-1 is boxed in red in the SDS-PAGE gel. The blue line is mAu at 280 nm and the green line is the sodium chloride concentration in mM.

Sodium chloride was used to elute any proteins bound to the resin, but no abFabI-1 was found in the eluted fractions. The protein could be aggregated, which would interfere with the way the protein interacts with the column.

Protein Separation by Hydrophobic Interaction Chromatography

Hydrophobic interaction chromatography (HIC) was used as another alternative to purify abFabI by separating the proteins by hydrophobicity. This type of chromatography uses ammonium sulfate to promote protein precipitation by having the protein compete with the salt for solvent, thus reducing the protein's solubility. We obtained pure, soluble abFabI from the HIC column (Figure 22), with a single band at the expected molecular weight for abFabI-1 of 35.8 kDa in the column's flow through. However, the abFabI-1 obtained from this column was not active according to the NADH consumption assay (data not shown).

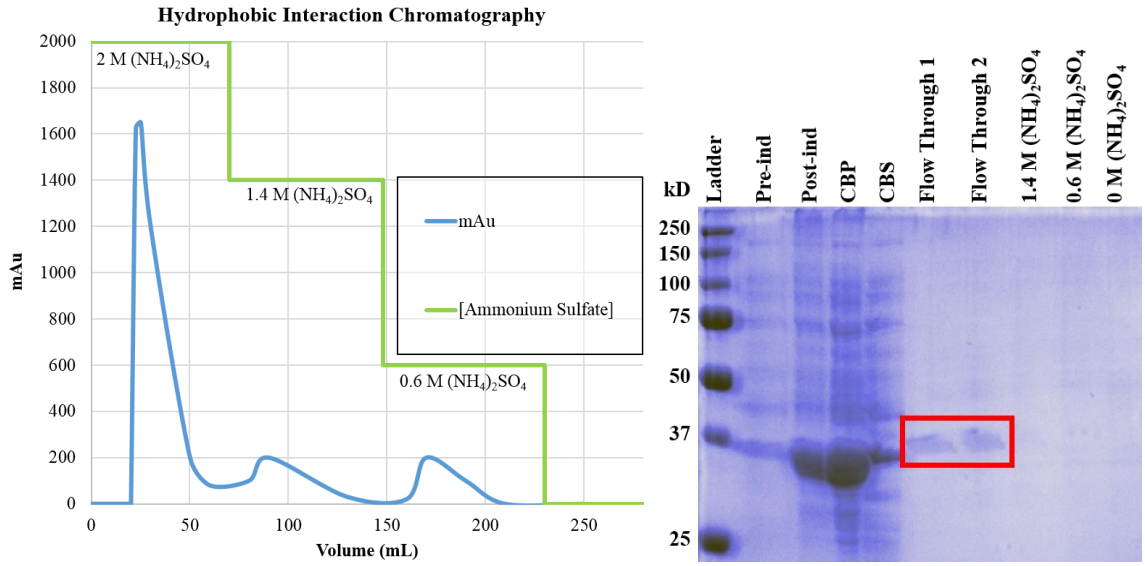

Figure 22: SDS-PAGE gel and UV trace for HIC. Top: SDS-PAGE gel. The single band that is predicted to be abFabI-1 appears in the first two flow through samples and is boxed in red. Bottom: UV trace for HIC. The blue line is mAu at 280 nm and the green line is the ammonium sulfate concentration in mM.

Protein Purification from Inclusion Bodies

Since the CBP contained a large amount of abFabI (Figure 17) and we had low yields of inactive protein when purifying from the supernatant, purifying from the inclusion bodies was a logical next approach to obtain pure, soluble, and active abFabI. Inclusion bodies contain proteins that have misfolded and remain as insoluble aggregates in the CBP; these misfolded proteins can be purified. Purification from inclusion bodies includes denaturation of the inclusion bodies and refolding of the protein of interest. After the pellet was denatured and refolded by rapid dilution, two molecular weight (MW) bands were seen on the SDS-PAGE gel (Figure 23).

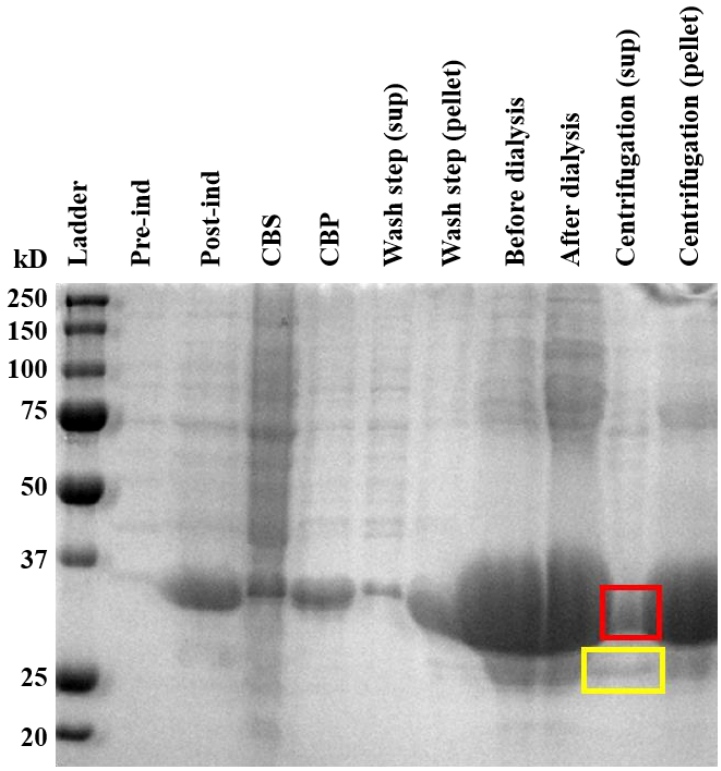

Figure 23: Purification of abFabI from the inclusion bodies. The pellet was washed, denatured, refolded, dialyzed, and centrifuged to obtain soluble protein. Folded protein is expected to be 36 kDa. A MW band at 32 kDa is boxed in red and another band at 27 kDa is boxed in yellow.

The two MW bands needed to be separated in order to obtain pure abFabI. Nickel affinity chromatography, size exclusion chromatography, ion exchange chromatography, and HIC were repeated with the refolded protein, but none of them were successful in providing usable abFabI. Since the previous chromatography columns were unsuccessful at purifying the desired abFabI, another type of chromatography column, HiTrap Blue HP column (which has an affinity resin), was used.

Protein Separation by Cibacron blue Affinity Chromatography

The HiTrap Blue HP column is a purification column that uses dye-ligand affinity chromatography, specifically using Cibacron blue, to separate the protein of interest from

unwanted proteins. Cibacron blue was expected to bind to abFabI-1 by mimicking NADH. Proteins bound to the HiTrap Blue HP column were expected to elute with increasing NADH concentrations. NADH can compete with Cibacron blue for the NADH binding site in abFabI-1 and thereby release protein from the column. The two MW bands refolded by rapid dilution were successfully separated by the dye-ligand affinity chromatography. A protein band of 32 kDa (abFabI-1H) was present in the flow through and another band of 27 kDa (abFabI-1L) was eluted starting with 2 mM NADH (Figure 24). This lower band was notable in that it had appeared in previous gels, did not correspond to any *E. coli* proteins based on our pre-induction culture samples, and seemed to be a degradation product or alternative form of abFabI-1 based on changes in band intensity with time or purification steps. The 32 kDa band will hereafter be referred to as "abFabI-1H" (H for "higher" MW band) and the 27 kDa band will be referred to as "abFabI-1L" (L for "lower" MW band).

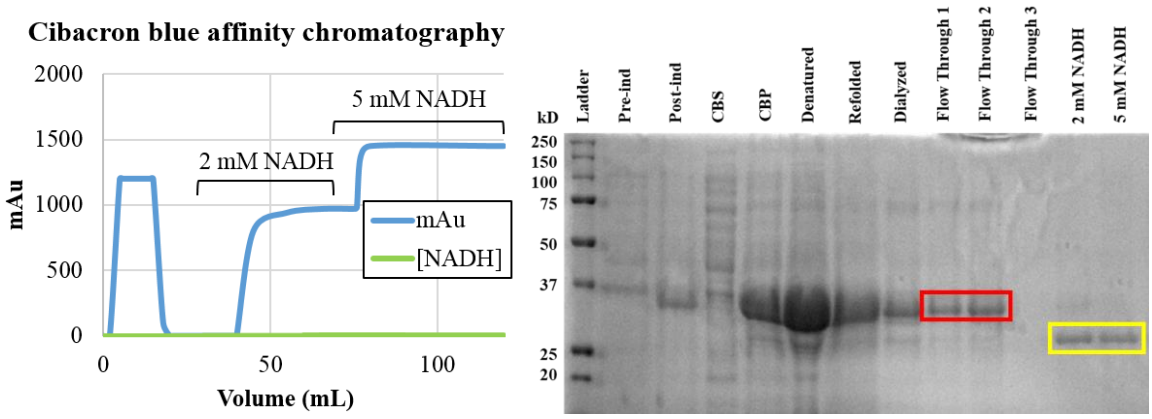

Figure 24: SDS-PAGE gel and UV trace for Cibacron blue affinity chromatography. The higher MW bands (32 kDa) from the flow through are boxed in red and the lower MW bands (27 kDa) eluted with 2 and 5 mM NADH are boxed in yellow. The blue line is mAu at 280 nm and the green line is the NADH concentration in mM.

Purification of abFabI-1 yielded active abFabI-1L

Both abFabI-1H and abFabI-1L were used in an NADH consumption assay to determine if the proteins were active (Figure 25).

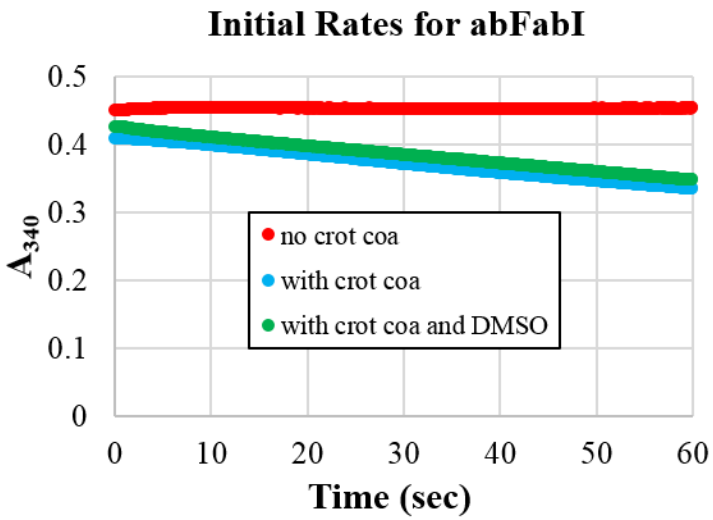

Figure 25: Raw data of NADH consumption assay. The initial rates for abFabI activity without substrate (red), with substrate (blue), and with substrate and DMSO (green) were obtained for specific activity calculations. abFabI-1H is not shown due to its inactivity and all three initial rates were done with abFabI-1L.

The initial rate, or the NADH consumption rate, is the slope of each line, which is used to calculate specific activity. Several control experiments were performed for the NADH consumption assay. First a no substrate (crotonyl-CoA) control was conducted to make sure that no NADH consumption occurs without substrate present to prove that any decreases in NADH absorbance observed in runs containing enzyme can be attributed to catalysis by abFabI. The enzyme was also tested with substrate in the presence of DMSO, the solvent later used to dissolve the inhibitors, to validate that abFabI activity is being inhibited by the inhibitors and not DMSO. No NADH is consumed in the absence of substrate, but in the presence of substrate, activity is seen, which means that NADH is only being converted to NAD^+ via active abFabI catalysis. The initial rates in the absence

or presence of DMSO are almost identical ($0.00130 \pm 8.04 \times 10^{-5}$ and $0.00128 \pm 1.32 \times 10^{-4}$ AU/min, respectively), which shows that DMSO does not affect the initial rate at the concentrations tested herein.

The calculations for the specific activity of abFabI are shown in the Materials and Methods. Table 12 shows the concentration, specific activity, and yield of abFabI-1 at various steps of the purification.

	Refolded abFabI-1 (before dialysis)	**Refolded abFabI-1 (after dialysis)**	**Eluted abFabI-1L (after dialysis)**
[abFabI] (mg/mL)	3.86	4.62	1.79
specific activity (μM/min·mg)	250	251	1886
yield (mg/L of growth)	42.5	50.8	2.15

Table 12: Protein concentration, specific activity, and yield of abFabI purified from the inclusion bodies.

By our NADH consumption assay, abFabI-1H was not active. The concentrations for abFabI-1 of 3.86 and 4.62 mg/mL were low after protein refolding. The column caused a loss of protein as well, reducing the concentration of the recovered abFabI-1L to 1.79 mg/mL due to the recovered abFabI-1 being split between a large amount of abFabI-1H and a lower quantity of abFabI-1L (Figure 24). The specific activity of abFabI was 250 μM/min·mg before dialysis and 251 μM/min·mg after dialysis. This suggests that dialysis did not affect the specific activity of the protein. After collecting the fractions containing abFabI-1L and dialyzing out the NADH, the pure abFabI-1L yielded a specific activity of 1886 μM/min·mg. Dye-ligand affinity chromatography had a purification factor of ~7.5 fold but only 4.23% of abFabI-1L was recovered from the column. The yield of 2.15 mg/L of growth after chromatography was extremely low compared to the refolded

protein yields of 42.5 and 50.8 mg/L of growth before chromatography. This decrease may also be due to the majority of the protein in that sample being abFabI-1H instead of the active abFabI-1L.

Differentiation of the two MW bands by Native PAGE

Identification of abFabI-1H and abFabI-1L were analyzed by native PAGE on a 12% polyacrylamide gel (Figure 26).

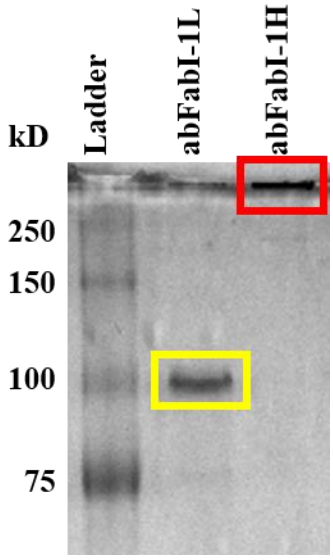

Figure 26: Native PAGE of the two abFabI samples. abFabI-1L at 100 kDa is boxed in yellow and abFabI-1H at the top of the gel is boxed in red.

abFabI-1H did not penetrate the gel and abFabI-1L migrated to 100 kDa. Since FabI from various bacterial species exhibit a homotetrameric native state, we expect abFabI to also be a homotetramer. According to the SDS-PAGE results, abFabI-1H is 32 kDa and abFabI-1L is 27 kDa, so the weight of the homotetramers should appear at 128 and 108 kDa, respectively. abFabI-1H may not be properly folded and in an aggregated state, which kept the protein from migrating through the gel, while abFabI-1L appeared to possibly be homotetrameric at 100 kDa, which only represents a 7.4% difference from

the expected molecular weight of 108 kDa. Based on the native gel results, it appears that abFabI-1L is the active and properly folded abFabI-1, while abFabI-1H appears to be misfolded and likely aggregated.

Identification of the two MW bands by Mass Spectrometry

Samples of both abFabI-1H and abFabI-L were sent to UCLA for mass spectrometry to determine their sequences. Each sample was digested with trypsin and chymotrypsin separately to obtain mass spectrometry data (Figure 27).

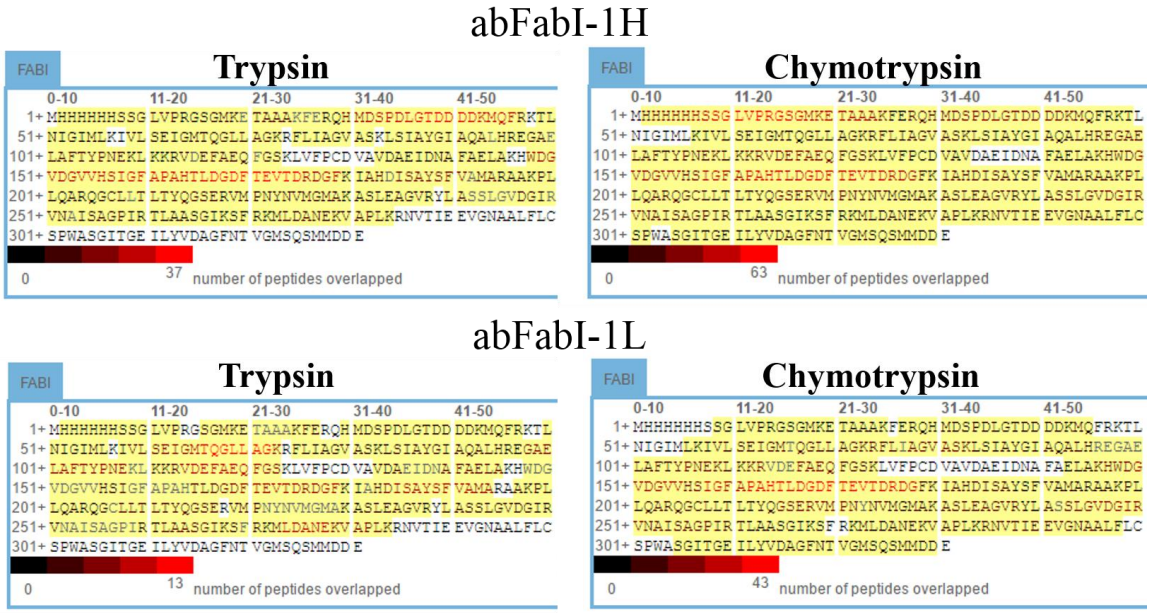

Figure 27: Mass spectrometry data of the two MW bands. The highlighted residues are residues confirmed with high confidence by mass spectrometry.

The data suggested that both MW bands share the same abFabI-1 sequence. It is still enigmatic how abFabI-1H and abFabI-1L have the same sequence even though their MW bands clearly migrated different distances on the SDS-PAGE gel (refer back to Figure 24). The percent difference between the inactive abFabI-1H and the expected abFabI-1 weight of 35.8 kDa is 10.6%, and the percent difference between abFabI-1L and abFabI-1

is 24.6%. Even though the proteins appear to be separate bands, the mass spectrometry data confirms that both bands are abFabI-1. SDS and heat may not successfully denature the structure of abFabI-1H or abFabI-1L, resulting in the MW difference observed. In other words, one gel form represents a fully unfolded species and the other species has retained some aspects of secondary structure (i.e. it is partially folded), giving rise to an aberrant gel mobility.

Inhibition Studies with abFabI-1L

We next wanted to determine the IC_{50} values of certain FabI inhibitors on abFabI activity. Inhibitors triclosan and diazaborines 14b, 18c, 35b, and 39 were all used in an attempt to inhibit the catalytic activity of the purified active abFabI-1L. Initial rates were quantitated by an NADH consumption assay to indirectly monitor the FabI catalyzed reduction of crotonyl CoA to butyryl CoA. The activity of abFabI was inhibited by triclosan with an IC_{50} value of 215 nM (Figure 28). This IC_{50} value for triclosan inhibition of abFabI is comparable to the other bacterial species (Table 13).

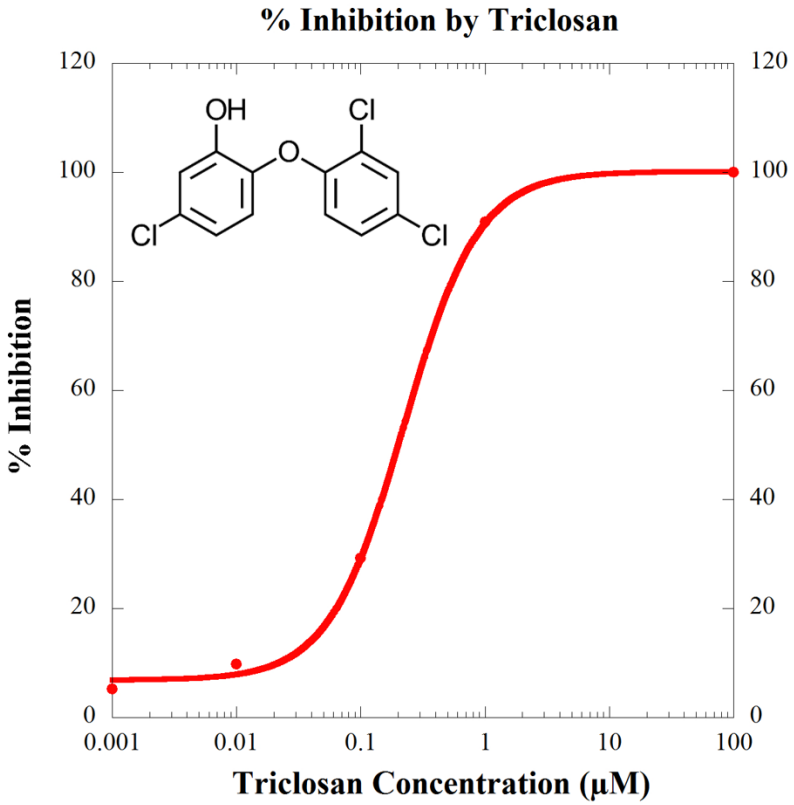
% Inhibition by Triclosan
% Inhibition
Triclosan Concentration (µM)
OH
Cl
O
Cl
Cl
120
100
80
60
40
20
0
0.001
0.01
0.1
1
10
100

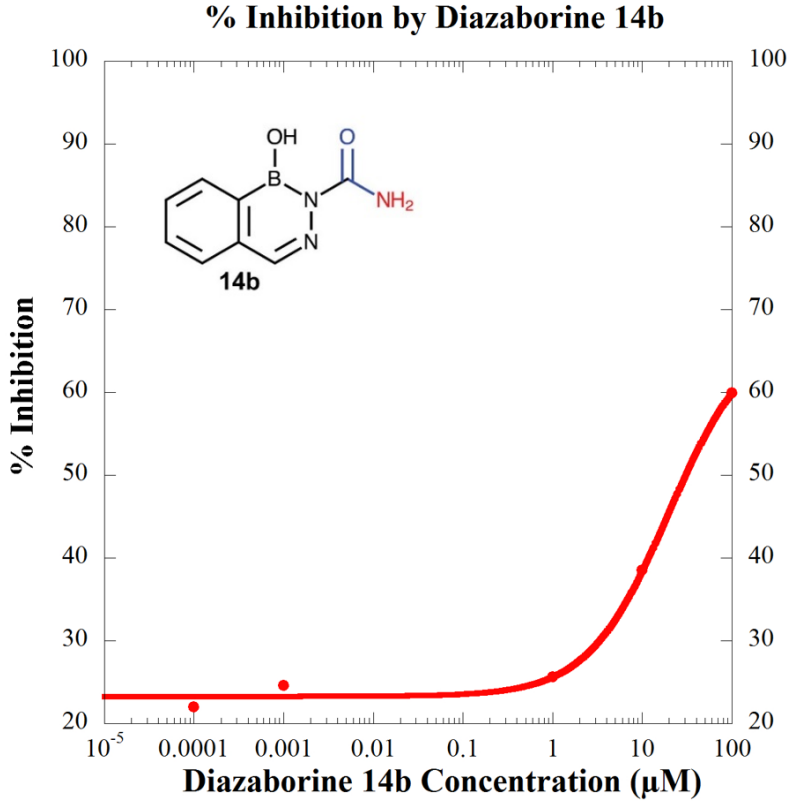
% Inhibition by Diazaborine 14b
% Inhibition
Diazaborine 14b Concentration (µM)
OH
B
N
N
O
NH2
14b
100
90
80
70
60
50
40
30
20
10-5
0.0001
0.001
0.01
0.1
1
10
100

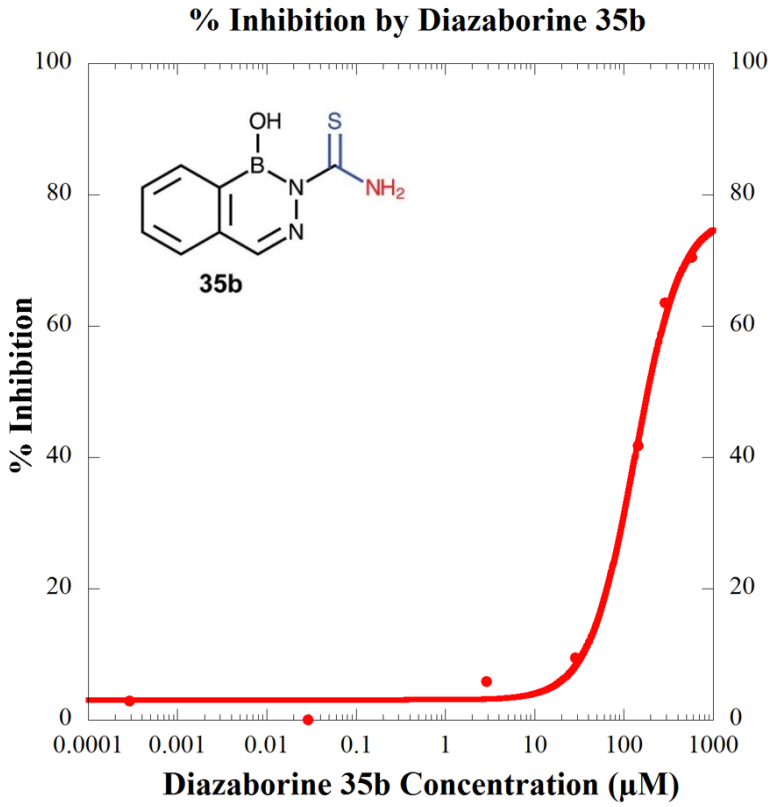
% Inhibition by Diazaborine 35b
% Inhibition
Diazaborine 35b Concentration (µM)
35b
OH
S
NH2
B
N
N
100
80
60
40
20
0
0.0001
0.001
0.01
0.1
1
10
100
1000

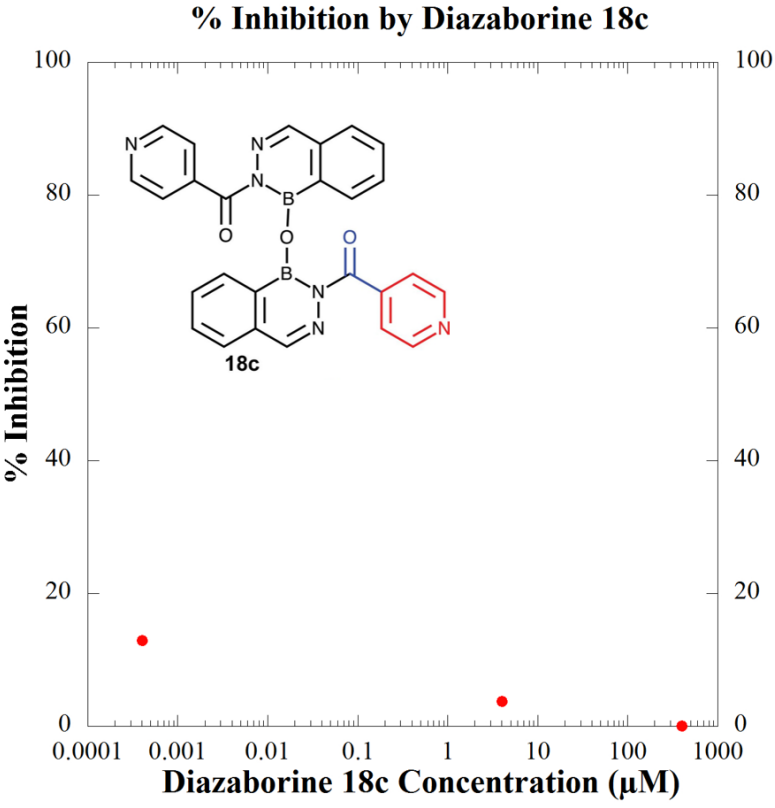
% Inhibition by Diazaborine 18c
% Inhibition
Diazaborine 18c Concentration (µM)
18c
N
O
B
100
80
60
40
20
0
0.0001
0.001
0.01
0.1
1
10
100
1000

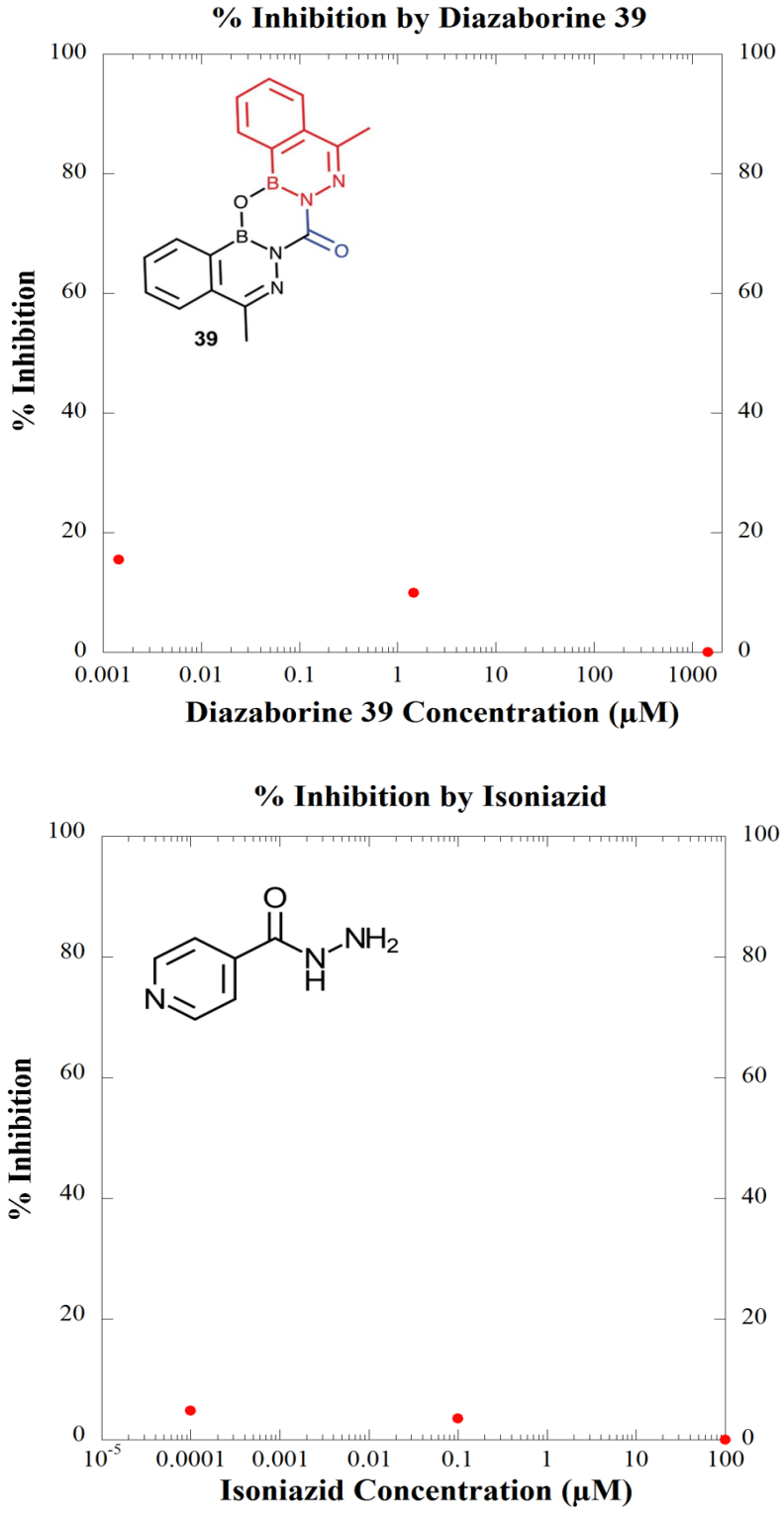

Figure 28: Percent inhibition of abFabI activity as a function of inhibitor concentration with abFabI-1L. IC_{50} plots of triclosan, diazaborines 14b, 35b, 18c, 39, and isoniazid.

Bacterial species	IC_{50} (μM)
A. baumannii	0.215
E. coli	0.04 [17]
M. tuberculosis	1 [33]
S. aureus	3 [20]

Table 13: IC_{50} values of triclosan on the FabI of various bacterial species. The IC_{50} of abFabI is highlighted in yellow above.

Triclosan is a submicromolar inhibitor of abFabI, which makes it a potent and useful compound for structure-based drug design. Diazaborines 14b and 35b had IC_{50} values of 11.9 and 122 μM, respectively (Figure 28). Even though these two diazaborines have lower potencies than triclosan, they still inhibit abFabI and can also be used for structure-based drug design. Isoniazid and diazaborines 18c and 39 did not inhibit abFabI activity (Figure 28). This could be due to the bulkiness of diazaborines 18c and 39, which may not fit into the active site of abFabI. Similarly, the isoniazid:NADH adduct, which is formed with KatG-activated isoniazid and NADH, may also be too bulky to fit into the abFabI active site. Since we did not activate isoniazid with KatG, we did not expect isoniazid to inhibit abFabI (Figure 28).

Subcloning to Improve Protein Solubility and Yield

Extra amino acids in the N-terminal insertion of the protein construct (red text of Figure 16 and bolded in Figure 29) may be the reason why the histidine tag was occluded and not binding to the nickel affinity chromatography column. This led us to subclone the abFabI gene into three new plasmids: pET-15b, pBG100, and pBG106. The shorter (referred to as abFabI-a) and longer (referred to as abFabI-b) versions of the abFabI gene

(Figure 29) were incorporated into each of the three new plasmids for a total of six protein constructs.

MQFRKTLNIGIMLKIVLSEIGMTQGLLAGKRFLIAGVASKLSIAYGIAQALHRE
GAELAFTYPNEKLKKRVDEFAEQFGSKLVFPCDVAVDAEIDNAFAELAKHWDG
VDGVVHSIGFAPAHTLDGDFTEVTDRDGFKIAHDISAYSFVAMARAAKPLLQAR
QGCLLTLTYQGSERVMPNYNVMGMAKASLEAGVRYLASSLGVDGIRVNAISAG
PIRTLAASGIKSFRKMLDANEKVAPLKRNVTIEEVGNAALFLCSPWASGITGEILY
VDAGFNTVGMSQSMMDDE

Figure 29: Protein sequences of abFabI-a and -b. abFabI-b includes an additional 21 amino acids (shown in bold) when compared to abFabI-a (not bolded).

Polymerase Chain Reaction

Primers were custom made and used in PCR experiments to amplify our desired insert DNA. The PCR product (insert DNA) is expected to have the abFabI gene sequence and restriction site sequences recognized by specific restriction enzymes. PCR products were extracted from an agarose gel (Figure 30a).

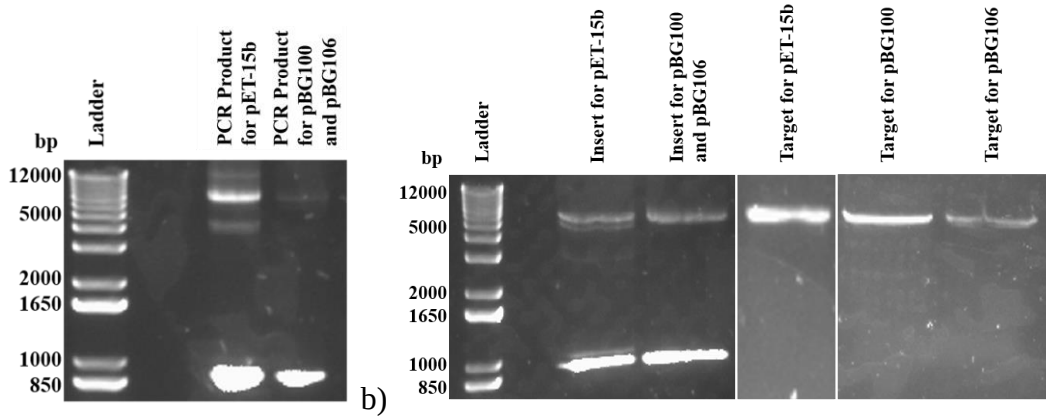

Figure 30: DNA agarose gels from subcloning. a) PCR products in pET-15b (870 base pairs) and the pBG plasmids (879 base pairs) b) Double digest products of the insert sequences for pET-15b (834 base pairs) and the pBG plasmids (843 base pairs) and target DNA sequences for pET-15b (5696 base pairs), pBG100 (5364 base pairs), and pBG106 (5388 base pairs).

Double Digestion and Ligation

The purified insert DNA and target plasmids were double digested by the appropriate restriction enzymes to yield cleaved products (Figure 30b). Double digested plasmids and inserts were ligated and transformed into *E. coli* to obtain the purified plasmid DNA for the six protein constructs. All six protein constructs were sequenced to confirm successful ligation.

Expression of abFabI with the pET-15b-abFabI Constructs

Out of the three plasmids, the two versions of abFabI in the pET-15b plasmid were selected for expression trials because the plasmid contains a 6xHis tag and a shorter linker compared to the pBG100 and pBG106 plasmids. Herein, the shorter abFabI in the pET-15b plasmid will be referred to as abFabI-2a and the longer abFabI in pET-15b will be referred to as abFabI-2b. Both versions were expressed at 18^{o}C and 37^{o}C (Figure 31).

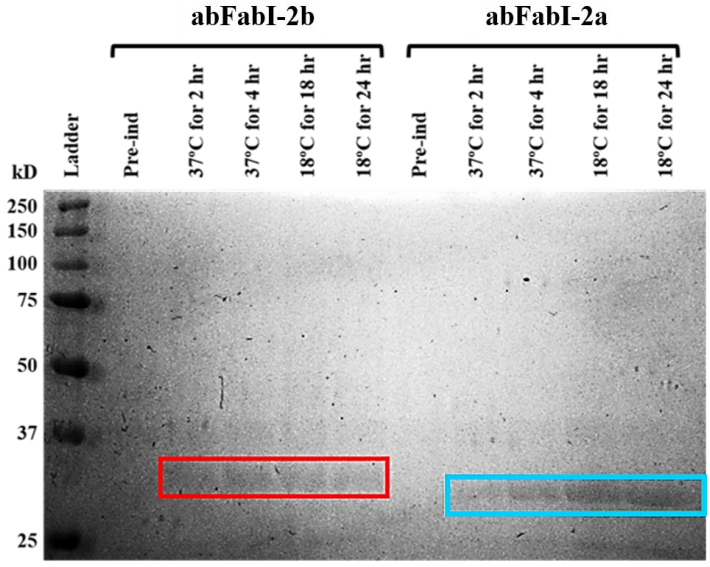

Figure 31: Expression of both versions of abFabI in the pET-15b plasmid. abFabI-2b is boxed in red at 33.2 kDa. abFabI-2a is boxed in blue at 30.8 kDa.

The proteins were successfully expressed at both temperatures. Based on intensity of the bands, a low amount of abFabI-2b was expressed as compared to abFabI-2a. Expressing abFabI-2a at 18°C seemed to yield more protein than at 37°C. Cells were lysed and the CBS and CBP of both versions were compared (Figure 32).

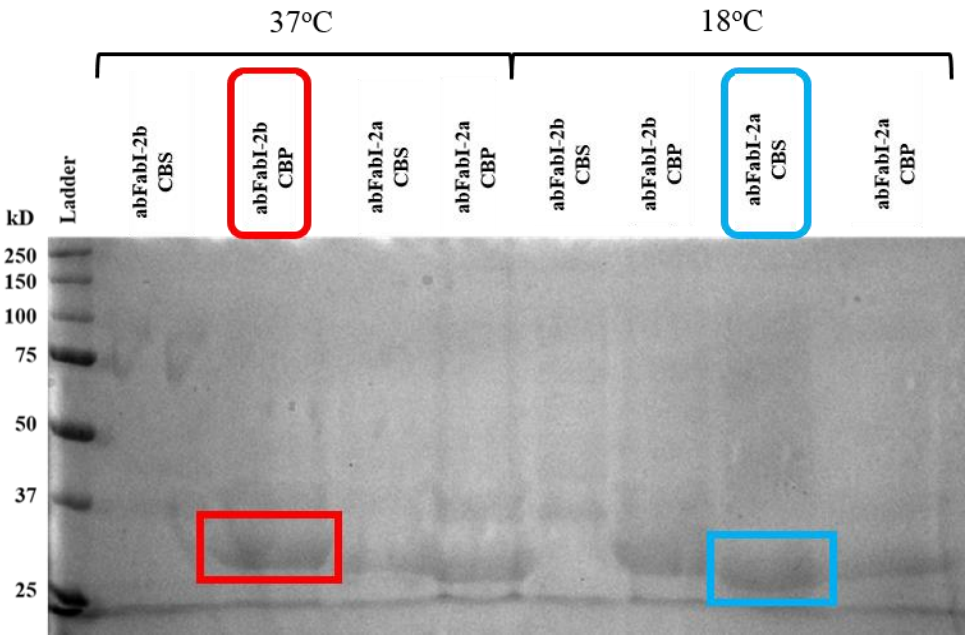

Figure 32: Protein expression in the CBS versus CBP. The colored boxes indicate the expression conditions and band for the abFabI-2b (red) and abFabI-2a (blue).

abFabI-2a was seen in the CBS and CBP for 18°C and 37°C. A large amount of soluble abFabI-2a was produced after 18 hours at 18°C; therefore, those conditions were used for purification. On the other hand, abFabI-2b was only seen in the CBP as appeared at both induction temperatures. No soluble abFabI-2b was produced. The CBP shows that a sufficient amount of protein was already produced after 4 hours at 37°C, so this condition would be used to produce insoluble abFabI-2b for purification from the inclusion bodies.

Purification of abFabI-2a by Nickel Affinity Chromatography

Soluble abFabI-2a needed to be separated from the native *E. coli* protein. Nickel affinity chromatography was performed on soluble abFabI-2a (Figure 33).

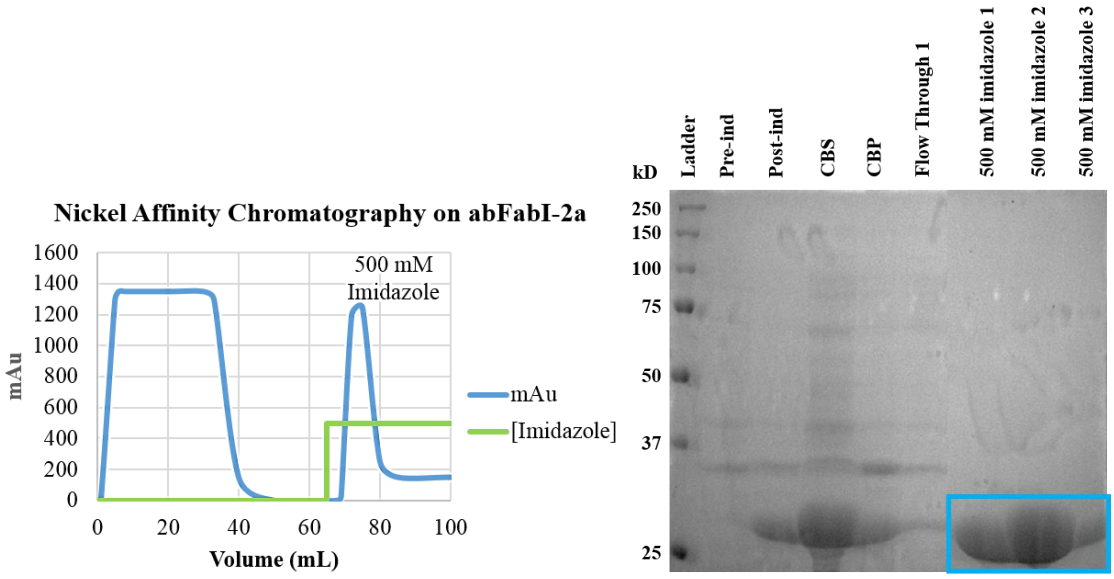

Figure 33: SDS-PAGE gel and UV trace for the purification of abFabI-2a by nickel affinity chromatography. abFabI-2a is boxed in blue. The blue line is mAu at 280 nm and the green line is the imidazole concentration in mM.

After the abFabI bound to the nickel-nitrilotriacetic acid (Ni-NTA) column via its 6xHis tag, pure protein was eluted off the column by 500 mM imidazole. Pure, soluble abFabI was shown to be active with a specific activity of 7497 µM/min·mg (Table 14). The concentration, specific activity, and yield of abFabI-2a were all significantly higher than abFabI-1L. Since the pure protein was active with a high protein concentration and yield, inhibition studies and eventual crystallization experiments can be performed to continue our progress on drug development through structure-based drug design.

	abFabI-1L	**abFabI-2a**
[purified abFabI]	1.79	38.6
specific activity (µM/min·mg)	1886	7497
yield (mg/L of growth)	2.15	50.2

Table 14: Concentration, activity, and yield of abFabI-1L and abFabI-2a.

Inhibition Studies with abFabI-2a

Inhibition studies were performed on abFabI-2a using the FabI inhibitors we had available in the lab. The IC_{50} values of triclosan, diazaborine 14b, and diazaborine 35b were determined to be 0.486, 5.81, and 173 µM, respectively (Figure 34). These IC_{50} values using abFabI-2a were comparable to the ones obtained with abFabI-1L (Table 15).

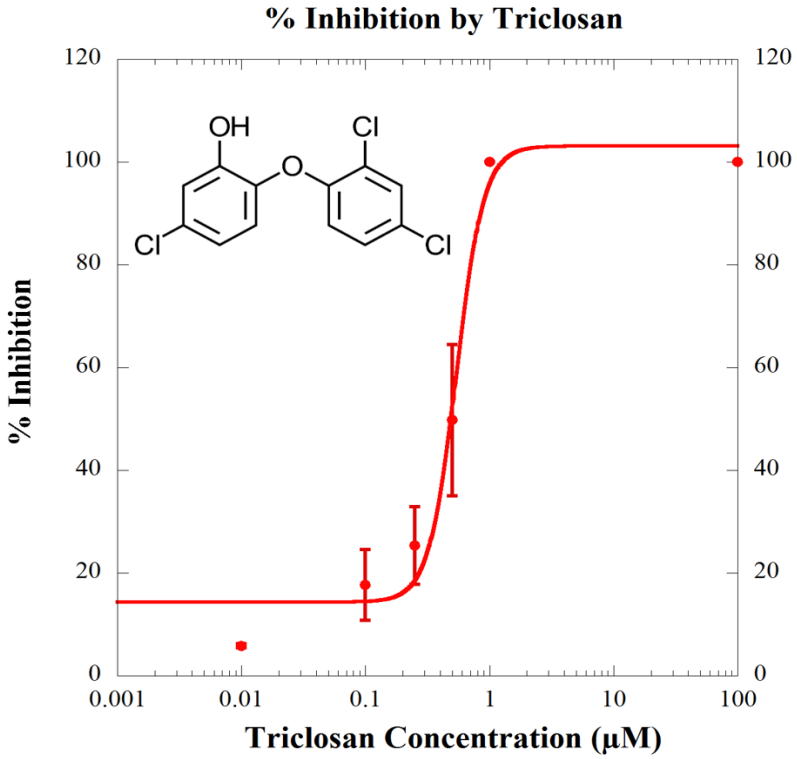

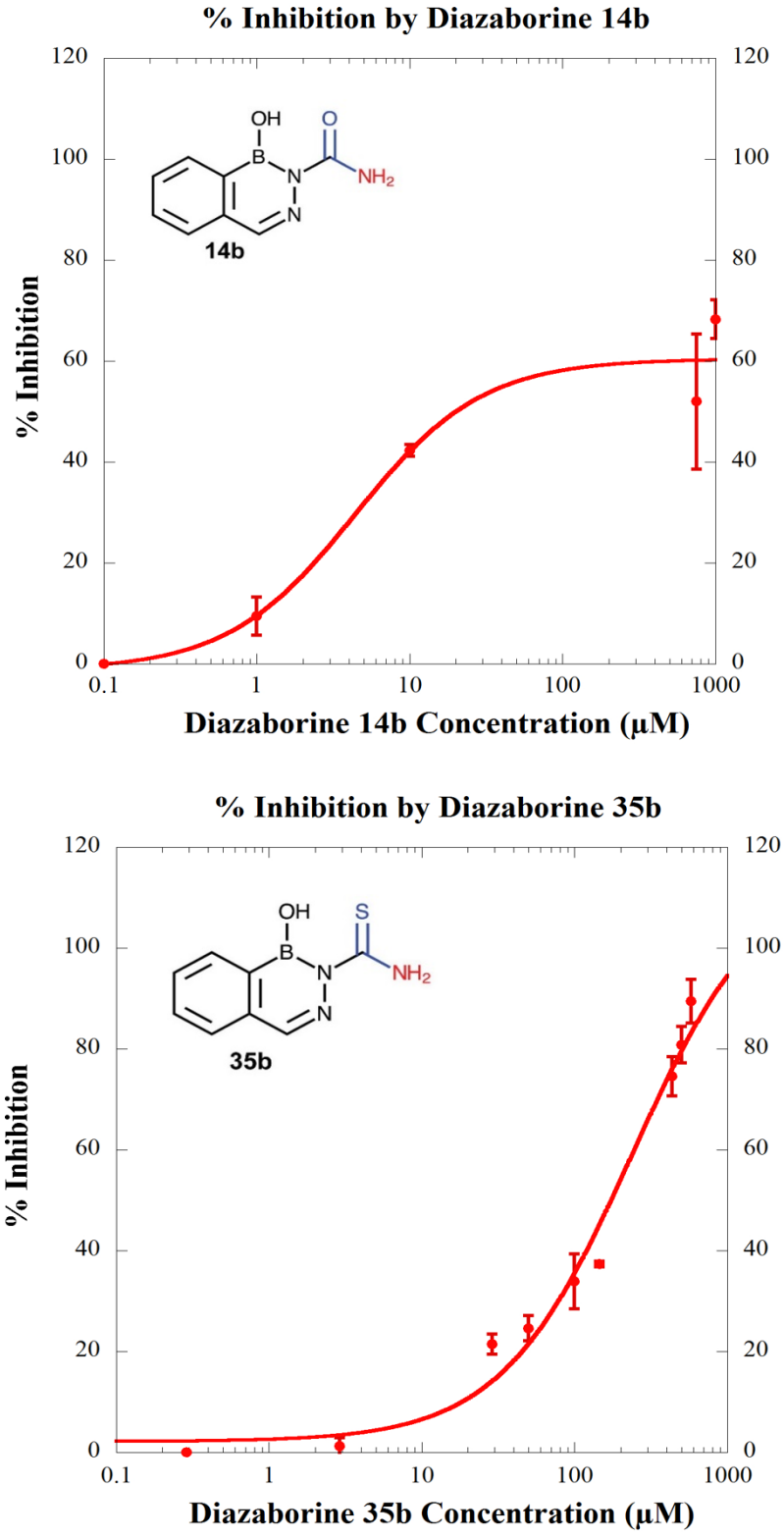

Figure 34: Percent inhibition of abFabI activity as a function of inhibitor concentration with abFabI-2a. Inhibition curves of triclosan, diazaborine 14b, and diazaborine 35b on abFabI.

	IC_{50} w/ triclosan	IC_{50} w/ diazab. 14b	IC_{50} w/ diazab. 35b
abFabI-2a	0.486 µM	5.81 µM	173 µM
abFabI-1L	0.215 µM	11.9 µM	122 µM

Table 15: Comparison of the IC_{50} values of FabI inhibitors on abFabI-2a and abFabI-1L.

The IC_{50} concentration for triclosan was once again in the submicromolar range and proves to be a potent inhibitor of abFabI. Complete abFabI inhibition is also seen at saturated concentrations, making triclosan an extraordinary abFabI inhibitor. Even though diazaborines 14b and 35b are not as potent as triclosan, the two diazaborine compounds are capable of inhibiting abFabI in the micromolar range. Diazaborine 14b is the least efficacious, only having a 60% maximum inhibition value, and diazaborine 35b reaches a maximum inhibition of 94%. In general, potency is the amount of drug needed to have a given effect and efficacy is the maximal effect of the drug. An inhibitor with high potency (low IC_{50}) and efficacy (high % inhibition) is desired. Triclosan fulfills both criteria as compared to the two diazaborines. Diazaborine 14b has a high potency but low efficacy, while diazaborine 35b has a low potency but high efficacy. Once again, these three inhibitors of abFabI activity can be used for structure-based drug design. Modifying these inhibitor structures can possibly lead to new therapeutics that inhibit abFabI activity with high efficacy and potency.

Discussion of the N-terminal Insertion in abFabI-b

abFabI-2a is the sequence found in 79% of the abFabI gene sequences registered in Uniprot and the only abFabI structure registered in the Protein Data Bank. It is the sequence used by many research groups, but there is a longer abFabI sequence, abFabI-b,

that is essentially abFabI-a with an N-terminal insertion of 21 amino acids (Figure 35). None of the structurally characterized FabI homologs have an equivalent N-terminal extension, so here, we hypothesize the purpose of this N-terminal insertion in abFabI-b, which is not known.

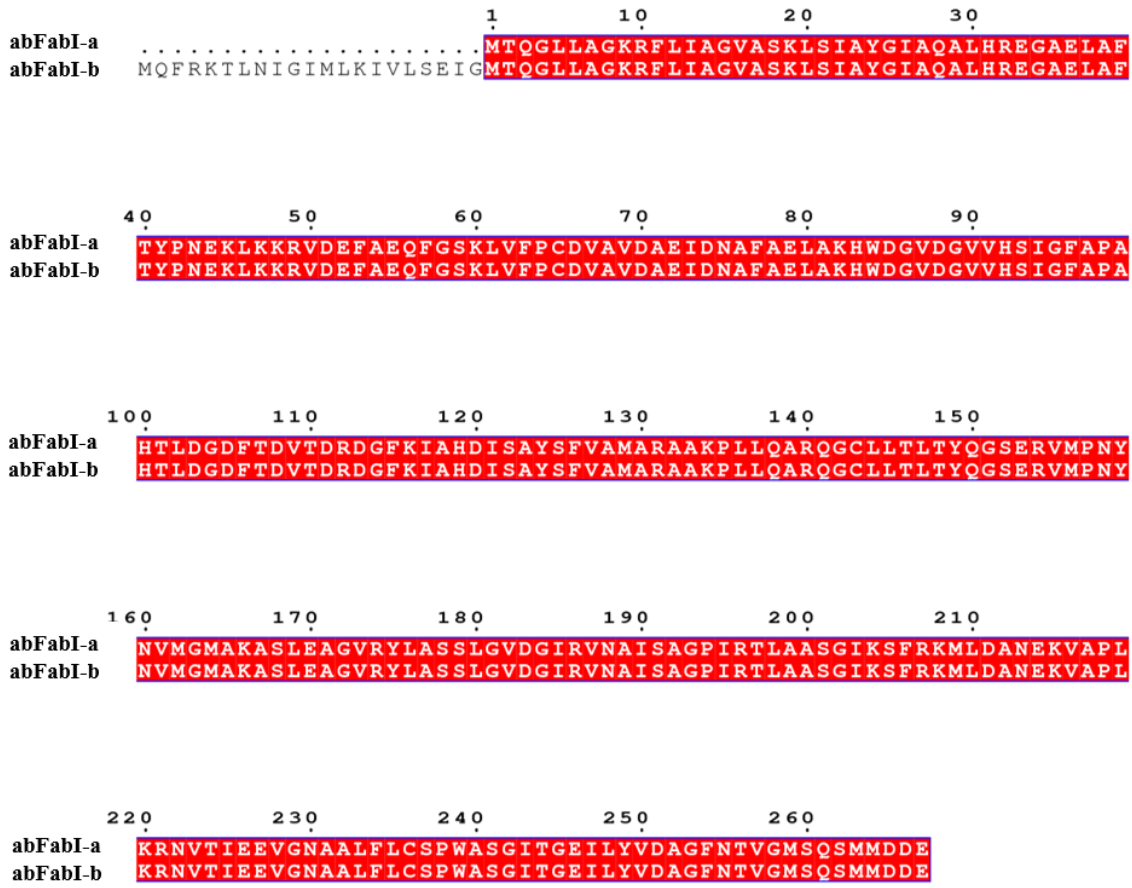

Figure 35: Sequence alignment of abFabI-a and abFabI-b. Identical residues are highlighted in red.[65]

This N-terminal insertion may play a biological role, such as translocation, tethering abFabI to the membrane, providing a post-translational modification site, or regulation enzyme activity. Perhaps the protein needs to travel between membranes or be near the membrane for the next reduction reaction to occur. No evidence has been shown that suggests abFabI translocates or needs to be tethered to the membrane for its catalytic

activity. This may require *in vivo* studies with abFabI to better understand the possibility of these two potential roles. The N-terminal sequence may be a post-translational modification site, so ExPASy tools (see Materials and Methods) were used to predict protein modification sites. Contrary to our hypothesis, none of the search engines predicted the abFabI sequence to have any of the following protein modification sites: palmitoylation, O- and N-glycosylation, oligosaccharide, phosphorylation, myristoylation, acetylation, glycation, sulfation, and sumoylation. Another possibility is that the N-terminal sequence is used for regulating the activity of the enzyme, such as the substrate binding loop that opens and closes depending on substrate or inhibitor binding. The enzyme could use the N-terminal sequence to control the catalytic activity in the FAS-II pathway to slow down or speed up fatty acid production. This would also require *in vivo* studies using abFabI. These are just some of the possible reasons for the N-terminal insertion, but more research needs to be done to elucidate this sequence that is problematic in purification and may not be needed. Other than these biological roles, the sequence may have a non-functional purpose.

A non-functional role of the N-terminal sequence is that it is an intron sequence. This possibility is unlikely though because no evidence has been shown that introns exist in *A. baumannii*. There could have also been a sequencing error in which the start of the sequence was defined incorrectly, leading to an extra 21 amino acids upon translation. The N-terminal that appears in abFabI-b may be a result of translating from the incorrect start codon, leading to two abFabI sequences. This theory is supported by the comparison of abFabI-2a and abFabI-2b expression (Figure 32). With just the difference of an N-terminal insertion of 21 amino acids, only insoluble abFabI-2b was produced with

pAbFabI-2b as compared to a large amount of soluble abFabI-2a produced with pAbFabI-2a. abFabI-2a includes the correct abFabI sequence, abFabI-a, which correlates with abFabI-2a being properly folded and yielding soluble and active protein. In contrast, abFabI-2b consists of abFabI-b, an incorrect sequence that includes the N-terminal insertion, leading to misfolding and solubility issues.

Conclusion and Future Direction

This work should assist in the major issue of battling against antibiotic resistance. We have successfully established a purification method for obtaining active and soluble abFabI and a method for inhibition studies. Two methods were able to yield the desired abFabI. The first method was performed with pAbFabI-1 and requires purification from inclusion bodies, protein refolding by rapid dilution, and protein separation by Cibacron blue affinity chromatography. This method yielded abFabI-1L that had high specific activity but low protein concentration and yield. The second method was simpler and only needed the soluble protein from lysed cells and protein separation by nickel affinity chromatography. We used pAbFabI-2a and purified abFabI-2a with significantly increased protein concentration, specific activity, and yield. The methods developed here can be used for obtaining abFabI for future experiments, such as crystallization. As a future direction, we want to structurally characterize abFabI with bound inhibitors. The solved structures of the inhibitor-bound abFabI can then be compared to abFabI alone for investigation of residues that can be exploited for developing narrow spectrum therapeutics.

Biochemical characterization is also important for pushing the research forward. Inhibition studies were completed by using an NADH consumption assay. Known FabI inhibitors were utilized in an attempt to inhibit the purified abFabI. IC_{50} values were acquired for abFabI inhibition by triclosan and diazaborines 14b and 35b. The values indicate that abFabI can indeed be inhibited by these compounds. Triclosan and diazaborines 14b and 35b can be used for structure-based drug design. The NADH consumption assay can be applied to other inhibitors to test for abFabI inhibition.

abFabI-2a was active and used in the inhibition studies. This activity implies that abFabI-a is the correct abFabI sequence out of the two abFabI gene sequences, abFabI-a and abFabI-b. The N-terminal insertion in abFabI-b has not been examined until now. abFabI-b may have been incorrectly sequenced, which led to the additional 21 amino acids at the N-terminal when compared to abFabI-a. The expression of abFabI-2b remaining in the insoluble portion of lysed cells supports the hypothesis that abFabI-b is misfolded and a result of sequencing error. Successful expression and purification of abFabI-2a from the soluble portion of lysed cells suggests that abFabI-a is the active and properly folded abFabI. Based on our results, abFabI-a should be the designated gene sequence used in experiments moving forward.

Bibliography

[1] Howard, A.; O'Donoghue, M.; Feeney, A.; Sleator, R.D. *Acinetobacter baumannii*: An emerging opportunistic pathogen. *Virulence*. **2012**, *3*, 243-250.

[2] Qureshi, N.N; Gallaher, B.; Schiller, N.L. Evolution of amoxicillin resistance of *Helicobacter pylori* in vitro: characterization of resistance mechanisms. *Microb. Drug. Resist.* **2014**, *20*, 509-516.

[3] Hum Nath Jnawali and Sungweon Ryoo. "First- and Second-Line Drugs and Drug Resistance." *Tuberculosis- Current Issues in Diagnosis and Management*. Ed. Bassam H. Mahboub. InTech, 2013.

[4] Engstrom, A.; Morcillo, N.; Imperiale, B.; Hoffner, S.; Jureen, P. Detection of First- and Second-Line Drug Resistance in *Mycobacterium tuberculosis* Clinical Isolates by Pyrosequencing. *J. Clin. Microbiol*. **2012**, *50*, 2026-2033.

[5] World Health Organization. WHO publishes list of bacteria for which new antibiotics are urgently needed. http://www.who.int/mediacentre/news/releases/2017/bacteria-antibiotics-needed/en/ (accessed March 16, 2017).

[6] Lu, H.; Tonge, P. Inhibitors of FabI, an Enzyme Drug Target in the Bacterial Fatty Acid Biosynthesis Pathway. *Acc. Chem. Res.* **2008**, *41*, 11-20.

[7] Maragakis, L.L.; Perl, T.M. *Acinetobacter baumannii*: Epidemiology, Antimicrobial Resistance, and Treatment Options. *Clin. Infect. Dis*. **2008**, *46*, 1254-1263.

[8] Peleg, A.Y.; Seifert, H.; Paterson, D.L. *Acinetobacter baumannii*: Emergence of a Successful Pathogen. *Clin. Microbiol. Rev.* **2008**, *21*, 538-582.

[9] Cunha, B.A. Optimal Therapy for Multidrug-Resistant *Acinetobacter baumannii*. *Emerg. Infect Dis.* **2010**, *16*, 170-171.

[10] Lehninger, A.L.; Nelson, D.L.; Cox, M.M. *Lehninger Principles of Biochemistry*. 6th ed., W.H. Freeman, **2013**, 833-839.

[11] Wright, H. T.; Reynolds, K. A. Antibacterial targets in fatty acid biosynthesis. *Curr. Opin. Microbiol*. **2007**, *10*, 447–453.

[12] Lu, X.; Huang, K.; You, Q. Enoyl acyl carrier protein reductase inhibitors: a patent review (2006-2010). *Expert Opin. Ther. Pat.* **2011**, *21*, 1007–1022.

[13] Massengo-Tiasse, R.P.; Cronan, J.E. Diversity in Enoyl-Acyl Carrier Protein Reductases. *Cell Mol. Life Sci.* **2009**, *66*, 1507-1517.

[14] Mistry, T.L.; Truong, L.; Ghosh, A.K.; Johnson, M.E.; Mehboob, S. Benzimidazole-Based FabI Inhibitors: A Promising Novel Scaffold for Anti-Staphylococcal Drug Development. *ACS Infect Dis.* **2017**, *3*, 54-61.

[15] Manjunatha, U.H.; Rao, S.; Kondreddi, R.R.; Noble, C.G.; Camacho, L.R.; Tan, B.H.; Ng, S.H.; Ng, P.S.; Ma, N.L.; Lakshminarayana, S.B.; Herve, M.; Barnes, S.W.; Yu, W.; Kuhen, K.; Blasco, F.; Beer, D.; Walker, J.R.; Tonge, P.J.; Glynne, R.; Smith, P.W.; Diagana, T.T. Direct inhibitors of InhA are active against *Mycobacterium tuberculosis*. *Sci. Transl. Med*. **2015**, *7*(*269*).

[16] Rafferty, J.B.; Simon, J.W.; Baldock, C.; Artymiuk, P.J.; Baker, P.J.; Stuitje, A.R.; Slabas, A.R.; Rice, D.W. Common themes in redox chemistry emerge from the X-ray structure of oilseed rape (*Brassica napus*) enoyl acyl carrier protein reductase. *Structure*. **1995**, *3*, 927-938.

[17] Dessen, A; Quémard, A.; Blanchard, J.S.; Jacobs, W.R., Jr.; Sacchettini, J.C. Crystal structure and function of the isoniazid target of *Mycobacterium tuberculosis*. *Science*. **1995**. *267*, 1638-1641.

[18] Stewart, M.J.; Parikh, S.; Xiao, G.; Tonge, P.J.; Kisker, C. Structural Basis and Mechanism of Enoyl Reductase Inhibition by Triclosan. *J. Mol. Biol*. **1999**, *290*, 859-865.

[19] Perozzo, R.; Kuo, M.; Sidhu, A.B.; Valiyaveettil, J.T.; Bittman, R.; Jacobs, W.R. Jr.; Fidock, D.A.; Sacchettini; J.C. Structural elucidation of the specificity of the antibacterial agent triclosan for malarial enoyl acyl carrier protein reductase. *J. Biol. Chem*. **2002**, *277*, 13106-13114.

[20] Chen, L.; Li, Y.; Ebihara, A.; Shinkai, A.; Kuramitsu, S.; Yokoyama, S.; Zhao, M.; Rose, J.P.; Wang, B.C. Crystal structure of Enoyl-[acyl-carrier-protein] reductase (NADH) from *Aquifex aeolicus* VF5. Southeast Collaboratory for Structural Genomics, RIKEN Structural Genomics/Proteomics Initiative, 2007.

[21] Tipparaju, S.K.; Mulhearn, D.C.; Klein, G.M.; Chen, Y.; Tapadar, S.; Bishop, M.H.; Yang, S.; Chen, J.; Ghassemi, M.; Santarsiero, B.D.; Cook, J.L.; Johlfs, M.; Mesecar, A.D.; Johnson, M.E.; Kozikowski, A.P. Design and synthesis of aryl ether inhibitors of the *Bacillus anthracis* enoyl-ACP reductase. *Chemmedchem*. **2008**, *3*, 1250-1268.

[22] Lee, H.H.; Moon, J.; Suh, S.W. Crystal structure of the *Helicobacter pylori* enoyl-acyl carrier protein reductase in complex with hydroxydiphenyl ether compounds, triclosan and diclosan. *Proteins*. **2007**, *69*, 691-694.

[23] Wang, F.; Langley, R.; Gulten, G.; Dover, L.G.; Besra, G.S.; Jacobs, W.R.; Sacchettini, J.C. Mechanism of thioamide drug action against tuberculosis and leprosy. *J. Exp. Med*. **2007**, *204*, 73-78.

[24] Kim, S.J.; Ha, B.H.; Kim, K.H.; Hong, S.K.; Shin, K.J.; Suh, S.W.; Kim, E.E. Dimeric and tetrameric forms of enoyl-acyl carrier protein reductase from *Bacillus cereus*. *Biochem. Biophys. Res. Commun.* **2010**, *400*, 517-522.

[25] Priyadarshi, A.; Kim, E.E.; Hwang, K.Y. Structural insights into *Staphylococcus aureus* enoyl-ACP reductase (FabI), in complex with NADP and triclosan. *Proteins.* **2010**, *78*, 480-486.

[26] Jiang, L.; Gao, Z.; Li, Y.; Wang, S.; Dong, Y. Crystal structures and kinetic properties of enoyl-acyl carrier protein reductase I from *Candidatus Liberibacter asiaticus*. *Protein Sci*. **2014**, *23*, 366-377.

[27] Lee, J.H.; Park, A.K.; Chi, Y.M.; Jeong, S.W. Crystal Structures of *Pseudomonas aeruginosa* Enoyl-ACP Reductase (FabI) in the Presence and Absence of NAD^+ and Triclosan. *Bull. Korean Chem. Soc.* **2015**, *36*, 322-326.

[28] Schiebel, J.; Chang, A.; Shah, S.; Lu, Y.; Liu, L.; Pan, P.; Hirschbeck, M.W.; Tareilus, M.; Eltschkner, S.; Yu, W.; Cummings, J.E.; Knudson, S.E.; Bommineni, G.R.; Walker, S.G.; Slayden, R.A.; Sotriffer, C.A.; Tonge, P.J.; Kisker, C. Rational design of broad spectrum antibacterial activity based on a clinically relevant enoyl-acyl carrier protein (ACP) reductase inhibitor. *J. Biol. Chem.* **2014**, *289*, 15987-16005.

[29] Yao, J.; Abdelrahman, Y.M.; Robertson, R.M.; Cox, J.V.; Belland, R.J.; White, S.W.; Rock, C.O. Type II Fatty Acid Synthesis Is Essential for the Replication of *Chlamydia trachomatis*. *J. Biol. Chem.* **2014**, *289*, 22365-22376.

[30] Abendroth, J.; Lorimer, D.D.; Edwards, T.E. Structure of a NADH-dependent enoyl-ACP reductase from *Acinetobacter baumannii* in complex with NAD. Seattle Structural Genomics Center for Infectious Disease (SSGCID), 2015.

[31] Bergler, H.; Wallner, P.; Ebeling, A.; Leitinger, B.; Fuchsbichler, S.; Aschauer, H.; Kollenz, G.; Högenauer, G.; Turnowsky, F. Protein EnvM is the NADH-dependent Enoyl-ACP Reductase (FabI) of *Escherichia coli*. *J. Biol. Chem.* **1994**, *269*, 5493-5496.

[32] Jordan, C.A.; Sandoval, B.A.; Serobyan, M.V.; Gilling, D.H.; Groziak, M.P.; Xu, H.H.; Vey, J.L. Crystallographic insights into the structure-activity relationships of diazaborine enoyl-ACP reductase inhibitors. *Acta. Crystallogr. F. Struct. Biol. Commun.* **2015**, *71*, 1521-1530.

[33] Ward, W.H.; Holdgate, G.A.; Rowsell, S.; McLean, E.G.; Pauptit, R.A.; Clayton, E.; Nichols, W.W.; Colls, J.G.; Minshull, C.A.; Jude, D.A.; Mistry, A.; Timms, D.; Camble, R.; Hales, N.J.; Britton, C.J.; Taylor, I.W. Kinetic and Structural Characteristics of the Inhibition of Enoyl (Acyl Carrier Protein) Reductase by Triclosan. *Biochemistry*. **1999**, *38*, 12514-12525.

[34] Heath, R.J.; Rubin, J.R.; Holland, D.R.; Zhang, E.; Snow, M.E.; Rock, C.O. Mechanism of Triclosan Inhibition of Bacterial Fatty Acid Synthesis. *J. Biol. Chem*. **1999**, *274*, 11110-11114.

[35] Baldock, C.; Rafferty, J.B.; Sedelnikova, S.E.; Baker, P.J.; Stuitje, A.R.; Slabas, A.R.; Hawkes, T.R.; Rice, D.W. A mechanism of drug action revealed by structural studies of enoyl reductase. *Science*. **1996**, *274*, 2107-2110.

[36] Baldock, C.; Rafferty, J.B.; Sedelnikova, S.E.; Bithell, S.; Stuitje, A.R.; Slabas, A.R.; Rice, D.W. Crystallization of *Escherichia coli* enoyl reductase and its complex with diazaborine. *Acta. Cryst.* **1996**, *52*, 1181-1184.

[37] Levy, C.W.; Roujeinikova, A.; Sedelnikova, S.; Baker, P.J.; Stuitje, A.R.; Slabas, A.R.; Rice, D.W.; Rafferty, J.B. Molecular basis of triclosan activity. *Nature*. **1999**, *398*, 383-384.

[38] Wagner, U.G.; Bergler, H.; Fuchsbichler, S.; Turnowsky, F.; Högenauer, G. Kratky, C. Crystallization and Preliminary X-ray Diffraction Studies of the Enoyl-ACP Reductase from *Escherichia coli*. *J. Mol. Biol*. **1994**, *243*, 126-127.

[39] Heath, R; Li, J.; Roland, G.E.; Rock, C.O. Inhibition of the *Staphylococcus aureus* NADPH-dependent enoyl-acyl carrier protein reductase by triclosan and hexchlorophene. *J. Biol. Chem.* **2000**, *275*, 4654-4659.

[40] de Boer, G.-J., Pielage, G. J. A., Nijkamp, H. J. J., Slabas, A. R., Rafferty, J. B., Baldock, C., Rice, D. W. and Stuitje, A. R. Molecular genetic analysis of enoyl-acyl carrier protein reductase inhibition by diazaborine. *Mol. Microbiol*. **1999**, *31*, 443–450.

[41] Baldock, C.; de Boer, G.J.; Rafferty, J.B.; Stuitje, A.R.; Rice, D.W. Mechanism of action of diazaborines. *Biochem. Pharmacol.* **1998**, *55*, 1541-1549.

[42] Levy, C.W.; Baldock, C.; Wallace, A.J.; Sedelnikova, S.; Viner, R.C.; Clough, J.M.; Stuitje, A.R.; Slabas, A.R.; Rice, D.W.; Rafferty, J.B. A Study of the Structure-Activity Relationship for Diazaborine Inhibition of *Escherichia coli* Enoyl-ACP Reductase. *J. Mol. Biol*. **2001**, *309*, 171-180.

[43] Kremer, L.; Dover, L.G.; Morbidoni, H.R.; Vilcheze, C.; Maughan, W.N.; Baulard, A.; Tu, S.C.; Honore, N.; Deretic, V.; Sacchettini, J.C.; Locht, C.; Jacobs, W.R.; Besra, G.S. Inhibition of InhA activity, but not KasA activity, induces formation of a KasA-containing complex in mycobacteria. *J. Biol. Chem.* **2003**, *278*, 20547-20554.

[44] Grassberger, M.A.; Turnowsky, F.; Hildebrandt, J. Preparation and antibacterial activities of new 1,2,3-diazaborine derivatives and analogs. *J. Med. Chem.* 1984, *27*, 947–953.

[45] Turnowsky, F.; Fuchs, K.; Jeschek, C.; Högenauer, G. envM genes of *Salmonella typhimurium* and *Escherichia coli*. *J. Bacteriol*. **1989**, *171*, 6555–6565.

[46] Kanichar, D.; Roppiyakuda, L.; Kosmowska, E.; Faust, M. A.; Tran, K. P.; Chow, F.; Buglo, E.; Groziak, M. P.; Sarina, E. A.; Olmstead, M. M.; Silva, I.; Xu, H. H. Synthesis, characterization, and antibacterial activity of structurally complex 2-acylated 2,3,1-benzodiazaborines and related compounds. *Chem. Biodivers*. **2014**, *11*, 1381-1397.

[47] Sullivan, T.J.; Truglio, J.J.; Boyne, M.E.; Novichenok, P.; Zhang, X.; Stratton, C.F.; Li, H.J.; Kaur, T.; Amin, A.; Johnson, F.; Slayden, R.A.; Kisker, C.; Tonge, P.J. High Affinity InhA Inhibitors with Activity against Drug-Resistant Strains of *Mycobacterium tuberculosis*. *ACS Chem. Biol.* **2006**, *1*, 43-53.

[48] Parikh, S.L.; Xiao, G.; Tonge, P.J. Inhibition of InhA, the Enoyl Reductase from *Mycobacterium tuberculosis*, Triclosan and Isoniazid. *Biochemistry*. **2000**, *39*, 7645-7650.

[49] Qiu, X.; Janson, A.; Court, R.I.; Smyth, M.G.; Payne, D.J.; Abdel-Meguid, S.S. Molecular basis for triclosan activity involves a flipping loop in the active site. *Protein Sci*. **1999**, *8*, 2529-2532.

[50] McMurry, L.M.; Oethinger, M.; Levy, S.B. Triclosan targets lipid synthesis. *Nature*. **1998**, *394*, 531-532.

[51] Parikh, S.; Moynihan, D. P.; Xiao, G.; Tonge, P. J. Roles of tyrosine 158 and lysine 165 in the catalytic mechanism of InhA, the enoyl-ACP reductase from *Mycobacterium tuberculosis*. *Biochemistry*. **1999**, *38*, 13623-13634.

[52] McMurry, L.M.; McDermott, P.F.; Levy, S.B. Genetic Evidence that InhA of *Mycobacterium Smegmatis* Is a Target for Triclosan. *Antimicrob. Agents Chemother*. **1999**, *43*, 711-713.

[53] Kuo, M.R.; Morbidoni, H.R.; Alland, D.; Sneddon, S.F.; Gourlie, B.B.; Staveski, M.M.; Leonard, M.; Gregory, J.S.; Janjigian, A.D.; Yee, C.; Musser, J.M.; Kreiswirth, B.; Iwamoto, H.; Perozzo, R.; Jacobs, W.R., Jr.; Sacchettini, J.C.; Fidock, D.A. Targeting Tuberculosis and Malaria through Inhibition of Enoyl Reductase. *J. Biol. Chem*. **2003**, *278*, 20851-20859.

[54] Xu, H.; Sullivan, T.J.; Sekiguchi, J.; Kirikae, T.; Ojima, I.; Stratton, C.F.; Mao, W.; Rock, F.L.; Alley, M.R.; Johnson, F.; Walker, S.G.; Tonge, P.J. Mechanism and Inhibition of saFabI, the Enoyl Reductase from *Staphylococcus aureus*. *Biochemistry*. **2008**, *47*, 4228-4236.

[55] Schiebel, J.; Chang, A.; Lu, H.; Baxter, M.V.; Tonge, P.J.; Kisker, C. *Staphylococcus aureus* FabI: inhibition, substrate recognition, and potential implications for in vivo essentiality. *Structure*. **2012**, *20*, 802-813.

[56] Park, H.S.; Yoon, Y.M.; Jung, S.J.; Kim, C.M.; Kim, J.M.; Kwak, J.H. Antistaphylococcal activities of CG400549, a new bacterial enoyl-acyl carrier protein reductase (FabI) inhibitor. *J. Antimicrob. Chemother.* **2007**, *60*, 568-574.

[57] Marrakchi, H.; Lanéelle, G.; Quémard, A. InhA, a target of the antituberculous drug isoniazid, is involved in a mycobacterial fatty acid elongation system, FAS-II. *Microbiology*. **2000**, *146*, 289-296.

[58] Johnsson, K.; Schultz, P.G. Mechanistic studies of the oxidation of isoniazid by the catalase peroxidase from *Mycobacterium tuberculosis*. *J. Am. Chem. Soc*. **1994**, *116*, 7425-7426.

[59] Lei, B.; Wei, C.J.; Tu, S.C. Action mechanism of antitubercular isoniazid. Activation by *Mycobacterium tuberculosis* KatG, isolation, and characterization of InhA inhibitor. *J. Biol. Chem*. **2000**, *275*, 2520-2526.

[60] Chollet, A.; Mourey, L.; Lherbet, C.; Delbot, A.; Julien, S.; Baltas, M.; Bernadou, J.; Pratviel, G.; Maveyraud, L.; Bernardes-Genisson, V. Crystal structure of the enoyl-ACP reductase of *Mycobacterium tuberculosis* (InhA) in the apo-form and in complex with the active metabolite of isoniazid pre-formed by a biomimetic approach. *J. Struct. Biol.* **2015**, *190*, 328-337.

[61] Banerjee, A.; Dubnau, E.; Quémard, A.; Balasubramanian, V.; Um, K.S.; Wilson, T.; Collins, D.; de Lisle, G.; Jacobs, W.R., Jr. inhA, a gene encoding a target for isoniazid and ethionamide in *Mycobacterium tuberculosis*. *Science*. **1994**, *14*, 227-230.

[62] Leung, E.T.Y.; Ho, P.L.; Yuen, K.Y.; Woo, W.L.; Lam, T.H.; Kao, R.Y.; Seto, W.H.; Yam, W.C. Molecular Characterization of Isoniazid Resistance in *Mycobacterium tuberculosis*: Identification of a Novel Mutation in *inhA*. *Antimicrob. Agents Chemother.* **2006**, *50*, 1075-1078.

[63] Basso, L. A.; Zheng, R.; Blanchard J. S. Mechanisms of Isoniazid Resistance in *Mycobacterium tuberculosis*: Enzymatic Characterization of Enoyl Reductase Mutants Identified in Isoniazid-Resistant Clinical Isolates. *J. Am. Chem. Soc.* **1998**, *118*, 11301-11302.

[64] Rawat, R.; Whitty, A.; Tonge, P.J. The isoniazid-NAD adduct is a slow, tight-binding inhibitor of InhA, the *Mycobacterium tuberculosis* enoyl reductase: Adduct affinity and drug resistance. *PNAS*. **2003**, *100*, 13881-13886.

[65] Robert, X.; Gouet, P.; Deciphering key features in protein structures with the new ENDscript server. *Nucleic Acids Research*. **2014**, *42*, 320-324.

[66] Šink, R.; Sosič, I.; Živec, M.; Fernandez-Menendez, R.; Turk, S.; Pajk, S.; Alvarez-Gomez, D.; Lopez-Roman, E.M.; Gonzales-Cortez, C.; Rullas-Triconado, J.; Angulo-Barturen, I.; Barros, D.; Ballell-Pages, L.; Young, R.J.; Encinas, L.; Gobec, S. Design, Synthesis, and Evaluation of New Thiadiazole-Based Direct Inhibitors of Enoyl Acyl Carrier Protein Reductase (InhA) for the Treatment of Tuberculosis. *J. Med. Chem*. **2015**, *58*, 613-624.

[67] Yao, J.; Zhang, Q.; Min, J.; He, J.; Yu, Z. Novel enoyl-ACP reductase (FabI) potential inhibitors of *Escherichia coli* from Chinese medicine monomers. *Bioorg. Med. Chem. Lett*. **2010**, *20*, 56-59.

[68] Takhi, M.; Sreenivas, K.; Reddy, C.K. Munikumar, M.; Praveena, K.; Sudheer, P.; Rao, B.N.; Ramakanth, G.; Sivaranjani, J.; Mulik, S.; Reddy, Y.R.; Narasimha, R.K.; Pallavi, R.; Lakshminarasimhan, A.; Panigrahi, S.K.; Antony, T.; Abdullah, I.; Lee, Y.K.; Ramachandra, M.; Yusof, R.; Rahman, N.A.; Subramanya, H. Discovery of azetidine based ene-amides as potent bacterial enoyl ACP reductase (FabI) inhibitors. *Eur. J. Med. Chem*. **2014**, *84*, 382-394.

[69] Tallorin, L.; Finzel, K.; Nguyen, Q.G.; Beld, J.; La Clair, J.J.; Burkart, M.D. Trapping of the Enoyl-Acyl Carrier Protein Reductase-Acyl Carrier Protein Interaction. *J. Am. Chem. Soc.* **2016**, *138*, 3962-3965.

[70] Garg, R.P.; Qian X.L.; Alemany L.B.; Moran.S.; Parry R.J. Investigations of valanimycin biosynthesis: elucidation of the role of seryl-tRNA. *Proc. Natl. Acad. Sci. U.S.A.* **2008**, *105*, 6543-6547.

Appendix

Purification of vlmH 7

As mentioned in the introduction, current antibiotics are becoming less effective on bacteria due to their evolving resistance. Besides inhibiting FAS-II pathway enzymes, like FabI, another option to fight against bacterial resistance is studying enzymes in pathways that synthesize therapeutic compounds, like valanimycin, an azoxy antibiotic that interferes with DNA synthesis and inhibits cell growth. Valanimycin is formed from the starting amino acid valine in the valanimycin biosynthetic pathway (Figure 36).

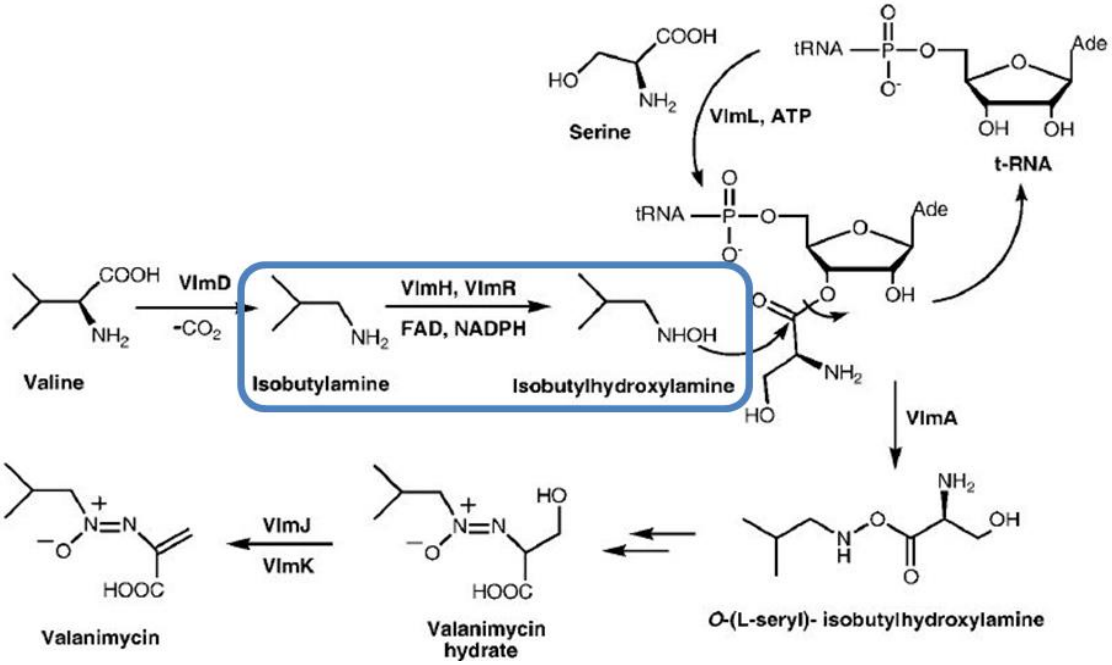

Figure 36: Valanimycin biosynthetic pathway. The reaction catalyzed by vlmH is boxed in blue.

Our lab focuses on the Class D flavin monooxygenase isobutylamine N-hydroxylase (vlmH), which catalyzes the reaction of isobutylamine to isobutylhydroxylamine in the pathway. By studying the structure and function of vlmH, metabolic engineering can be achieved. Even though the long term goal is to solve the structure of vlmH by X-ray

diffraction for antibiotic development, soluble and active enzyme needs to be expressed and purified beforehand. The vlmH from *Streptomyces viridifaciens* (vlmH1) was successfully purified in our lab (Charmaine Ibarra, CSUN) and the significance and background can be found in her thesis work. We obtained sequence homologs of vlmH1 (Table 16). Here, the purification of vlmH7, which is the vlmH from *Streptomyces viridochromogenes*, is presented.

Homolog	Organism	ID to vlmH	pET15b construct MW
vlmH1	*Streptomyces viridifaciens*	100.0%	
vlmH2	*Streptomyces sp. WM6378*	86.5%	42357.0
vlmH3	*Streptomyces sp. WM6378*	82.6%	42218.8
vlmH4	*Kitasatospora setae NBRC 14216* (aka *Streptomyces setae*)	72.8%	41990.8
vlmH5	*Kitasatospora setae NBRC 14216* (aka *Streptomyces setae*)	61.4%	42028.6
vlmH6	*Streptomyces sp. NRRL WC-3618*	60.3%	41297.0
vlmH7	*Streptomyces viridochromogenes*	59.8%	41668.2

Table 16: Structural homologs of vlmH.

The vlmH7 protein construct is shown in Figure 36. A 6xHis tag in the protein construct is used to purify vlmH7 by nickel affinity chromatography.

MGSSHHHHHHSSGLVPRGSH**MRSLTTAREVCERHQPGLLAALESLSFAEREA TGSPAVARLREHGGAGLLVPVEYGGQGADVLDAVRVQRAVGAVSPSLAAA STMHHFTVAMLFELATDASRLTPAQTKVLHGIAPERLLLASGWAEGRTQQN ILIPSVTATETEGGFLLNGAKKPCSLARSMDVLTASIAVPGADGTPELALALL PADSPGLSVHPFWGNEVLAASESEEVRLTDVFVPQELVVRTVPEAPHLLDDL QTTGFVWFELLICAGYAGAATALAATVLERGRGSSGERAALAVRVESAFAL LEGAARAVRDGLDGEAAVAEVLVARYAAQETLVQAADQALDLLGGIDFVR GGEHTRLADSVRPLVFHPPGRASAAEPLLQWFAGGALELS**

Figure 37: **Protein construct sequence of vlmH7 in pET-15b**. vlmH7 is bolded. The construct has 399 amino acids and weighs 41.7 kDa.

Both the lysis and binding buffers consisted of 50 mM Tris-Cl and 500 mM NaCl at pH 7.5, and the elution buffer contained 50 mM Tris-Cl, 500 mM NaCl, and 500 mM imidazole at pH 7.5. Since pure, soluble, and active enzyme is desired, the cell break supernatant, which is the soluble form, was used for the nickel affinity chromatography. After vlmH7 bound to the nickel resin and was separated from other unwanted proteins, at least 100 mM imidazole was needed to elute vlmH7 of 41.7 kDa (Figure 37).

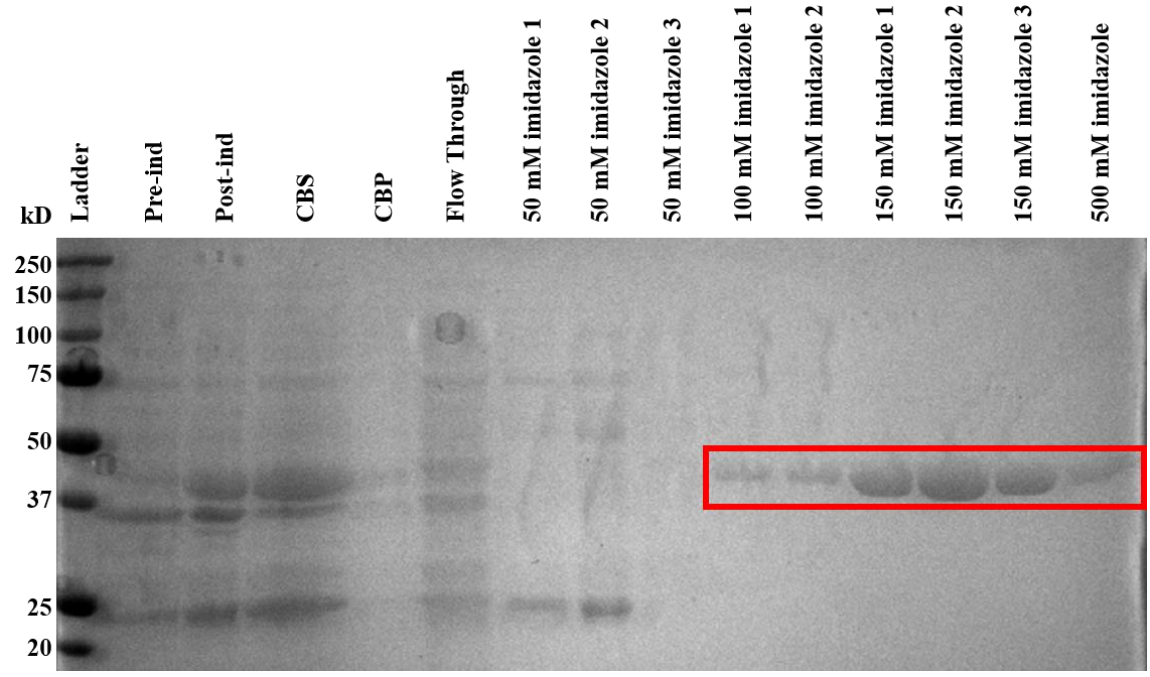

Figure 38: **Purification of vlmH7 by nickel affinity chromatography**. Pure bands of vlmH7 are boxed in red.

The oligomeric state and activity of the successfully purified enzyme vlmH7 needs to be analyzed. After confirming that the vlmH7 is active, further studies, like crystallization experiments, can be performed to progress towards the eventual goals of structural characterization and metabolic engineering for antibiotic development.